

• Master's Programme in Computer, Communication and Information Sciences

Wideband Channel Estimation for OFDM Systems: A Carrier Aggregation and Interpolation Approach

Jingtao Zhong

Copyright ©2025 Jingtao Zhong

Author	Jingtao Zhong		
Title of thesis	Wideband Channel Estimation for OFDM Systems: A Carrier Aggregation and Interpolation Approach		
Programme	Computer, Communication and Information Sciences		
Major	Communications Engineering		
Thesis supervisor	Prof. Risto Wichman		
Thesis advisor(s)	Prof. Risto Wichman		
Date	16.04.2025	Number of pages	59
		Language	English

Abstract

With the increased demand for high-speed wireless communications and accurate wireless positioning, the requirement for wideband communication systems is becoming higher. One of the core modules to ensure the reliable communication is the channel estimation. Channel estimation is also an essential prerequisite for carrier-aggregated positioning system. While traditional CA-based channel estimation methods only utilize the narrowband responses of individual carriers, the frequency gaps between them remain unutilized, leading to suboptimal performance.

This thesis investigates a wideband channel estimation method that relies on non-contiguous carrier aggregation. The proposed approach constructs the wideband channel estimate by leveraging narrowband measurement from each carrier component and applying interpolation algorithms. A phase correction algorithm is also proposed to solve the problem of phase discontinuity in multiple narrowband measurements. This thesis evaluates the wideband channel estimation algorithm by MATLAB simulation, comparing different interpolation techniques in terms of estimation accuracy and computational efficiency while demonstrating the feasibility of the proposed approach.

Keywords Channel Estimation, Carrier Aggregation, OFDM, Phase Discontinuity

Table of contents

Preface and acknowledgements	6
Symbols and abbreviations.....	7
Symbols	7
Operators.....	7
Abbreviations	7
1 Introduction	9
2 Basis of OFDM Carrier Aggregation System.....	11
2.1 Wireless Multipath Channel Analysis	11
2.1.1 Multipath Propagation Channel	11
2.1.2 Multipath Fading.....	12
2.1.3 Channel Correlation Properties.....	13
2.2 OFDM Transmission in Wireless Systems	18
2.3 Carrier Aggregation Technology Overview.....	21
2.3.1 Carrier Aggregation Classification	21
2.3.2 Carrier Aggregation Deployment Scenarios	22
2.4 Channel Estimation	23
2.4.1 Least Square Algorithm.....	24
2.4.2 MMSE Algorithm.....	25
2.4.3 DFT-Based Channel Estimation Algorithm	26
3 Wideband Channel Estimation Framework	28
3.1 Problem Formulation.....	28
3.1.1 Channel Estimation in Carrier Aggregation Systems	28
3.1.2 Phase Discontinuity in Carrier Aggregation Systems	29
3.1.3 General Structure of Wideband Channel Estimation	30
3.2 Phase Offset Correction	32
3.3 Interpolation for Wideband Channel Reconstruction	35
3.3.1 Linear Interpolation	35
3.3.2 Spline Interpolation.....	36
3.3.3 Kriging Interpolation.....	39
4 Simulation Results and Performance Evaluation.....	42
4.1 Simulation Setup.....	42

4.1.1	Channel Generation	42
4.1.2	Signal Transmission and Reception.....	44
4.1.3	Wideband Channel Estimation Implementation.....	44
4.2	Covariance Matrix Generation for Kriging Interpolation	44
4.2.1	Monte Carlo Method	45
4.2.2	Method based on Gaussian Process Regression Model.....	45
4.3	Selection of Suitable Number of Sample Points for Interpolation	46
4.3.1	Interpolation of Perfect Channel Estimate	47
4.3.2	Interpolation of Imperfect Channel Estimate.....	48
4.4	Performance of Wideband Channel Estimation.....	49
4.4.1	Phase Offset Correction.....	50
4.4.2	Overall Performance Analysis	52
5	Conclusions and Future Work	55
5.1	Conclusions	55
5.2	Future Work.....	55
	References.....	56

Preface and acknowledgements

I would like to express my sincere gratitude to Professor Risto Wichman for his valuable advice and guidance throughout this work.

I am also grateful to the friends I made during my studies in Finland and the colleagues I had the pleasure of working with during my internship at NXP in Shanghai.

Finally, I would like to thank my parents for their unwavering support throughout my studies.

Otaniemi, 13 March 2025

Jingtao Zhong

Symbols and abbreviations

Symbols

$\mathbb{C}^{M \times N}$	Set of $M \times N$ complex value matrices
I	Identity matrix

Operators

A^T	Transpose of matrix A
A^H	Hermitian transpose of matrix A
A^{-1}	Inversion of matrix A
$\mathbb{E}[\cdot]$	Ensemble Average which is applied to stochastic processes, or the mean of random variables
$\ \cdot\ _2$	Euclidean norm
Δf	Difference of function f
$\frac{d}{dt}$	derivative with respect to the variable t
$\angle f$	Phase value of function f
\circ	Element-wise multiplication

Abbreviations

CA	Carrier Aggregation
OFDM	Orthogonal frequency-division multiplexing
FFT	Fast Fourier Transform
IFFT	Inverse Fast Fourier Transform
DFT	Discrete Fourier Transform
LS	Least Square
MMSE	Minimum Mean Square Error
MSE	Mean Square Error
LO	Local Oscillator
PLL	Phase-locked Loop
RF	Radio Frequency
ISI	Inter-Symbol Interference

SNR	Signal-to-noise ratio
GPR	Gaussian Process Regression
TDL	Tap Delay Line

1 Introduction

In recent years, with the development of information and communication technologies, people's demand for various communication services and the requirements for communication quality have increased. In addition, providing accurate positioning information is also vital for the next generation communication systems. In communication systems, greater bandwidth translates to faster data transmission and higher positioning accuracy. To support wireless systems with a bandwidth beyond 20MHz, Orthogonal frequency-division multiplexing (OFDM) and Carrier Aggregation technologies (CA) were introduced and adopted in 4G mobile networks [1].

Orthogonal frequency division multiplexing (OFDM) has become one of the essential technologies in mobile communication systems since the 4G LTE (Long-term Evolution) era owing to its ability to mitigate multipath fading and achieve high spectral efficiency [2]. However, with the increasing demand for higher data rates, OFDM systems with a single frequency band can no longer meet the requirements. In addition, spectrum scarcity for wireless communication is also a notable challenge [3].

Carrier aggregation (CA) is one of the key features of LTE-Advanced to make full use of spectrum resources. CA refers to the use of discrete spectrum resources together to transmit data on multiple frequency bands, thereby increasing the data transmission speed [3]. In an OFDM-based carrier aggregation system, both the number of utilized frequency bands and the specific bands selected can vary to meet complex communication requirements [4]. High accuracy positioning in 5G and beyond is also a key motivation for CA, as CA effectively increases the available bandwidth for Time-of-Arrival (TOA) estimation [5].

In order to enable reliable and high-speed data transmission, the receiver needs to perform channel estimation, which is used to estimate the channel response so that the receiver can accurately restore the original data information [6]. In high accuracy wireless positioning systems, wideband channel estimation is a critical prerequisite for the TOA estimation. However, directly measuring a large contiguous bandwidth channel requires wideband receivers, which introduces significant challenges in hardware design and cost efficiency [7][8]. [5] proposed a method to improve positioning accuracy by using carrier aggregation, where the method relies on independently processing each narrowband component in CA. If a continuous wideband channel response is constructed based on known narrowband components, the available bandwidth for TOA estimation can be increased, thereby supporting more accurate positioning for 5G and beyond.

One possible approach to perform wideband channel estimation without a wideband receiver is to use multiple narrowband carriers. This idea is particularly well-suited for non-contiguous CA systems, where narrowband channel estimates of each carrier component are known. Then, the interpolation algorithms are employed to fill in the gaps to construct the full wideband channel response.

Numerous studies [9][10][11] investigated channel estimation algorithms for a single frequency band. In [12][13][14], multi-band OFDM channel estimation was studied, which shares similarities with contiguous CA systems. Channel estimation for contiguous CA systems was investigated in [15]. However, no studies have focused on wideband channel estimation of non-contiguous CA systems. Based on the previous, the objective of this thesis is to design the wideband channel estimation algorithm for the OFDM-based carrier aggregation system. For this purpose, this thesis uses MATLAB to develop a wideband channel estimation simulation platform. The simulation code includes the signal reception and transmission, wideband channel estimation algorithm implementation, and effect verification. In addition, to ensure the efficiency of the algorithm, this thesis compares different interpolation techniques and optimizes the computational resources needed according to the error of channel estimation.

The rest of this thesis is organized as follows. Chapter 2 introduces the fundamental concepts of OFDM, multipath channels, carrier aggregation, and channel estimation techniques. Chapter 3 presents the framework of wideband channel estimation algorithm, including phase offset correction and interpolation techniques. Chapter 4 describes the structure of the simulation platform and discusses the performance of the wideband channel estimation algorithm. Chapter 5 provides the conclusion of the thesis and outlines potential directions for future research.

2 Basis of OFDM Carrier Aggregation System

2.1 Wireless Multipath Channel Analysis

This section will focus on the wireless channel of the mobile communication system. In wireless communication, signals are transmitted in the form of radio waves, and the space through which the signal passes from the transmitter to the receiver is called the wireless channel. Since the wireless channel may change randomly at any time, the signal will be affected by the change of the wireless channel during the transmission process of the wireless channel. Therefore, it is very important to study the transmission characteristics of the channel and establish the corresponding channel model.

2.1.1 Multipath Propagation Channel

Multipath propagation in wireless communications refers to the signal propagating from transmitter to receiver through multiple paths due to reflections, diffractions, and scattering in the transmission environment [2]. The arrival time, attenuation and phase of signals propagating from different paths are different at the receiving end. Define the frequency of the transmitted signal as ω and the received signal as $E_z(\omega, t)$. $E_z(\omega, t)$ is the combination of multiple waves, and its expression is as follows.

$$E_z(\omega, t) = E_0 \sum_{n=1}^N \sum_{m=1}^M C_{nm} \cos(\omega t + \omega_n t - \omega T_{nm}) \quad (1)$$

$E_0 C_{nm}$ is the amplitude coefficient of each path component, and C_{nm} are normalized with an ensemble average equal to 1. ω is the Angular frequency of the transmitted signal. ω_n represents the Doppler shift, resulting from the relative motion between the transmitter and the receiver. There are N different paths, and the signal of each path consist of M components with different propagation delays T_{nm} .

The power of each individual wave: C_{nm}^2 can be expressed as:

$$C_{nm}^2 = G(\alpha_n) p(\alpha_n, T_{nm}) dadT \quad (2)$$

where $G(\alpha_n)$ is the horizontal directivity pattern of the receiving antenna, which describes the characteristics of the receiving antenna's ability to receive signals at different horizontal angles α_n . $p(\alpha_n, T_{nm})$ refers to the distribution of power over time and angle, so $p(\alpha_n, T_{nm}) dadT$ represents the

proportion of incident power within a small angle interval $d\alpha$ around angle α and within a short time interval dT around time T .

For simplicity, in this thesis, we assume a uniform distribution in the angle of the incident power α , and there is no antenna directivity:

$$p(\alpha, T) = \frac{1}{2\pi} e^{-\frac{T}{\sigma}} \quad (3)$$

$$G(\alpha) = 1 \quad (4)$$

Where τ is a measure of time delay spread, which will be introduced in section 2.1.2.

Therefore, by substituting (3) and (4) into (2), we obtain:

$$C_{nm}^2 = p(\alpha_n, T_{nm}) d\alpha dT = \frac{1}{2\pi} e^{-\frac{T_{nm}}{\tau}} d\alpha dT \quad (5)$$

2.1.2 Multipath Fading

Fading refers to the distortion of the signal at the time domain or frequency domain, which can degrade communication reliability. The two main sources of channel amplitude deterioration are additive noise and fading. The Gaussian white noise channel model is a typical additive noise, and the fading channel causes multiplicative signal disturbances.

In multipath propagation, the coherent combination of multiple signals from different paths at the receiving end causes variations in signal strength. These variations exhibit a high degree of randomness, leading the wireless signal to undergo dramatic fluctuations during transmission in a very short period or a very short distance. Multipath propagation gives rise to this phenomenon, which is referred to as multipath fading. Multipath fading can lead to two special selective fading: time-selective fading and frequency-selective fading. Time-selective fading distorts the received signal in the time domain, while frequency-selective fading distorts the signal in the frequency domain.

In wideband communication systems, the impact of frequency selective fading is more significant. Due to the wide channel bandwidth, the different path delay components generated by multipath propagation are usually distinguishable. The time difference between signals from different paths in a multipath channel arriving at the receiver is called delay spread. Delay spread is a critical parameter that characterizes the dispersion of the channel. A common measure of delay spread is the maximum delay spread. It is expressed as:

$$\tau = \tau_{max} - \tau_{min} \quad (6)$$

where τ_{max} and τ_{min} represent the maximum and minimum propagation delays T_{nm} in equation (1). Root mean square (RMS) delay spread is a more comprehensive measure of delay spread, which is given by:

$$\tau_{rms} = \sqrt{\frac{\sum C_{nm}^2 (T_{nm} - \bar{\tau})^2}{\sum C_{nm}^2}} \quad (7)$$

Where C_{nm}^2 is the received power of each path component, and $\bar{\tau}$ is the mean propagation delay:

$$\bar{\tau} = \frac{\sum C_{nm}^2 \tau_{nm}}{\sum C_{nm}^2} \quad (8)$$

When the delay spread is large, the signals of different frequency components experience varying degrees of interference, resulting in some frequency components being enhanced while others are depressed. The frequency response of the channel is no longer flat, some frequency components will be severely attenuated, while others may be enhanced. This is frequency selective fading.

The different time delays in multipath propagation cause the statistical properties of signals at different frequencies to become uncorrelated when the frequency separation exceeds the coherence bandwidth of the channel. Coherence bandwidth refers to the frequency interval for which the signals are still strongly correlated. If the frequency interval of two frequency components is less than the coherence bandwidth, they are correlated and have similar fading characteristics. If their frequency interval is greater than the coherence bandwidth, they are no longer correlated and no longer have the same fading characteristics [16].

2.1.3 Channel Correlation Properties

By studying the correlation coefficient as a function of frequency separation, we can determine the coherence bandwidth over which the phase response remains consistent [17]. In CA systems, potential usage of the channel correlation function includes analysis of the cell coverage, channel state estimation and the frequency diversity gain [18]. In this thesis, understanding the correlation properties of the channel is critical for the wideband channel estimation system design, which will be introduced in Chapter 4. Therefore, in this section, we will investigate the phase correlation functions based on the channel model in 2.1.1.

$E_z(\omega_1, t)$ and $E_z(\omega_2, t)$ are two narrow band signals received at frequencies ω_1 and ω_2 :

$$\begin{aligned} E_z(\omega_1, t) &= x_1(t) \cos \omega_1 t - x_2(t) \sin \omega_1 t \\ E_z(\omega_2, t) &= x_3(t) \cos \omega_2 t - x_4(t) \sin \omega_2 t \end{aligned} \quad (9)$$

where $x_1(t)$ and $x_3(t)$ are the in-phase component of $E_z(\omega_1, t)$ and $E_z(\omega_2, t)$. $x_2(t)$ and $x_4(t)$ are the quadrature component.

According to the central limit theorem, when N and M are large enough, $x_i(t)$ are Gaussian random processes and they are jointly Gaussian distributed.

So, $x_i(t)$ can be expressed as:

$$\begin{aligned} x_1(t) &= E_0 \sum_{n,m} C_{nm} \cos(\omega_n t - \omega_1 T_{nm}) \\ x_2(t) &= E_0 \sum_{n,m} C_{nm} \sin(\omega_n t - \omega_1 T_{nm}) \\ x_3(t) &= E_0 \sum_{n,m} C_{nm} \cos(\omega_n t - \omega_2 T_{nm}) \\ x_4(t) &= E_0 \sum_{n,m} C_{nm} \sin(\omega_n t - \omega_2 T_{nm}) \end{aligned} \quad (10)$$

Define frequency separation as s . Define four random variables x_1, x_2, x_3, x_4 for fixed time t .

$$s = \omega_2 - \omega_1 \quad (11)$$

$$x_i \triangleq x_i(t) \quad i = 1, 2, 3, 4 \quad (12)$$

Then, the amplitude and phase can be defined as:

$$\begin{aligned} x_1 &\triangleq r_1 \cos \theta_1 \\ x_2 &= r_1 \sin \theta_1 \\ x_3 &\triangleq r_2 \cos \theta_2 \\ x_4 &= r_2 \sin \theta_2 \end{aligned} \quad (13)$$

The statistical characteristics are determined by moments of the form $E[x_i x_j]$.

$$\mathbb{E}[x_i x_j] = E_0^2 \sum_{n,m,p,q} \langle C_{nm} C_{pq} \cos(\omega_n t - \omega_i T_{nm}) \cos(\omega_p t - \omega_j T_{pq}) \rangle \quad (14)$$

where $i, j = 1, 2, 3, 4$

When $i = j$, this implies that $C_{nm} = C_{pq}$ leading to the following result:

$$\mathbb{E}[x_i^2] = \frac{E_0^2}{2} \sum_{n,m} C_{nm}^2 = b_0 \sum_{n,m} \frac{1}{2\pi} e^{-\frac{T}{\tau}} d\alpha dT \quad (15)$$

where $b_0 = \frac{E_0^2}{2}$ is the mean power.

In the limit as $N, M \rightarrow \infty$:

$$\begin{aligned} \mathbb{E}[x_i^2] &= b_0 \int_0^{2\pi} \int_0^\infty e^{-\frac{T}{\tau}} d\alpha dT, i = 1, 2, 3, 4 \\ &= b_0 \end{aligned} \quad (16)$$

Similarly, through the operation of trigonometric functions and the properties of the ensemble average, we get

$$\begin{aligned} \mathbb{E}[x_1 x_3] &= b_0 \int_0^{2\pi} \int_0^\infty \frac{1}{2\pi} e^{-\frac{T}{\tau}} \cos(sT) dT d\alpha \\ &= b_0 \frac{1}{1 + s^2 \tau^2} \end{aligned} \quad (17)$$

$$\begin{aligned} \mathbb{E}[x_1 x_4] &= b_0 \int_0^{2\pi} \int_0^\infty \frac{1}{2\pi} e^{-\frac{T}{\tau}} \sin(-sT) dT d\alpha \\ &= -\frac{b_0 s \tau}{1 + s^2 \tau^2} \end{aligned} \quad (18)$$

The in-phase and quadrature components are statistically uncorrelated, so when $i = 1, j = 2$ or $i = 3, j = 4$:

$$\mathbb{E}[x_1 x_2] = \mathbb{E}[x_3 x_4] = 0 \quad (19)$$

According to the properties of joint Gaussian variable, and applying the transformation of variables in (13), the joint density of the envelopes and phases $p(r_1, r_2, \theta_1, \theta_2)$ can be expressed as:

$$p(r_1, r_2, \theta_1, \theta_2) = \frac{r_1 r_2}{(2\pi\mu)^2(1-\lambda^2)} \exp\left[-\frac{r_1^2 + r_2^2 - 2r_1 r_2 \lambda \cos(\theta_2 - \theta_1 - \phi)}{2\mu(1-\lambda^2)}\right] \quad (20)$$

where

$$\tan\phi = \frac{\mu_2}{\mu_1}, \quad \lambda^2 = \frac{\mu_1^2 + \mu_2^2}{\mu^2} \quad (21)$$

$$\mu = \mathbb{E}[x_1^2], \quad \mu_1 = \mathbb{E}[x_1 x_3], \quad \mu_2 = \mathbb{E}[x_1 x_4] \quad (22)$$

By substituting (17), (18) and (19) into (21) and (22), we obtain the expression of $\tan\phi$ and λ , which will be used for the expression of phase correlation properties expression:

$$\tan\phi = -s\tau \quad (23)$$

$$\lambda = \frac{1}{1 + s^2\tau^2} \quad (24)$$

By integrating expression (20), we can get the joint distribution of two phases [16]:

$$\begin{aligned} p(\theta_1, \theta_2) &= \int_0^\infty \int_0^\infty p(r_1, r_2, \theta_1, \theta_2) dr_1 dr_2 \\ &= \frac{1 - \lambda^2 \sqrt{1 - B^2} + B \cos^{-1}(-B)}{4\pi^2 (1 - B^2)^{3/2}} \end{aligned} \quad (25)$$

$$B = \lambda \cos(\theta_2 - \theta_1 - \phi), \quad 0 < \cos^{-1}(-B) < \pi \quad (26)$$

The correlation of two phases can be expressed as:

$$R_\theta(s) = \mathbb{E}[\theta_1 \theta_2] = \int_0^{2\pi} \int_0^{2\pi} \theta_1 \theta_2 p(\theta_1, \theta_2) d\theta_1 d\theta_2 \quad (27)$$

Integration by parts yields a simple series expansion [16]:

$$R_\theta(s) = \pi^2 \left[1 + \Gamma(\lambda, \phi) + 2\Gamma^2(\lambda, \phi) - \frac{1}{24}\Omega(\lambda) \right] \quad (28)$$

$$\Gamma(\lambda, \phi) = \frac{1}{2\pi} \sin^{-1}(\lambda \cos \phi) \quad (29)$$

$$\Omega(\lambda) = \frac{6}{\pi^2} \sum_{n=1}^{\infty} \frac{\lambda^{2n}}{n^2} \quad (30)$$

The phases of two signals θ_1 and θ_2 are random variables uniformly distributed from zero to 2π . Thus:

$$p(\theta) = \frac{1}{2\pi} \quad (31)$$

Mean value of θ_1 , θ_2 , θ_1^2 , and θ_2^2 are:

$$\begin{aligned} \mathbb{E}[\theta_1] &= \mathbb{E}[\theta_2] = \pi \\ \mathbb{E}[\theta_1^2] &= \mathbb{E}[\theta_2^2] = \frac{4\pi^2}{3} \end{aligned} \quad (32)$$

The correlation coefficient of the phase:

$$\rho_{\theta}(s) = \frac{R_{\theta}(s, \tau) - \mathbb{E}[\theta_1]\mathbb{E}[\theta_2]}{\sqrt{(\mathbb{E}[\theta_1^2] - \mathbb{E}[\theta_1]^2)(\mathbb{E}[\theta_2^2] - \mathbb{E}[\theta_2]^2)}} = \frac{3}{\pi^2} [R_{\theta}(s) - \pi^2] \quad (33)$$

Substituting (28) into (33):

$$\rho_{\theta}(s) = 3\Gamma(\lambda, \phi)[1 + 2\Gamma(\lambda, \phi)] - \frac{1}{8}\Omega(\lambda) \quad (34)$$

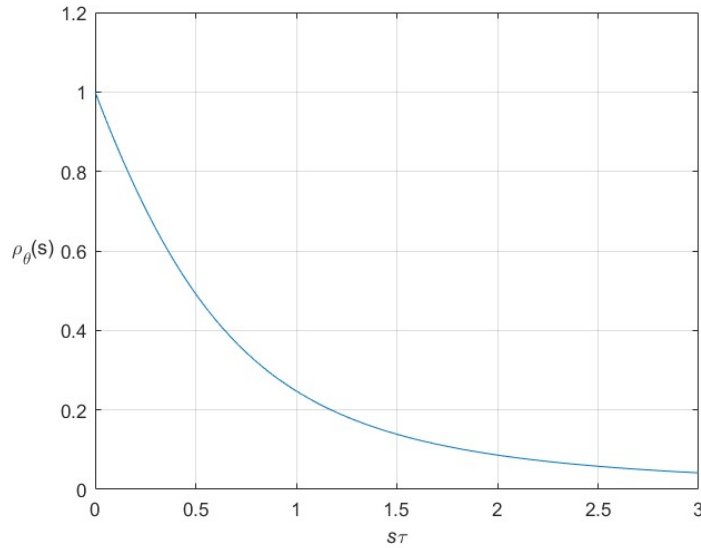


Figure 1. Dependence of the phase correlation coefficient on the frequency separation s and time delay spread τ

The relationship between the phase correlation coefficient and $s\tau$ is illustrated in Figure 1. If we define coherence bandwidth as the frequency interval $\rho_\theta(s) = 0.5$, this condition is met when $s\tau = 0.5$, which results in a coherence bandwidth of $0.25\pi\sigma$. Therefore, the expression of coherent bandwidth can be:

$$B_c = \frac{1}{4\pi\tau} \quad (35)$$

This approximation indicates that a larger delay spread leads to a smaller coherence bandwidth. It is because, when the delay spread is large, multipath components are more dispersed in time, causing rapid variations in the channel frequency response. Consequently, the coherence bandwidth becomes smaller, implying that signals with a bandwidth greater than B_c will experience frequency-selective fading.

2.2 OFDM Transmission in Wireless Systems

According to Shannon's information theory, channel capacity increases as bandwidth increases, so increasing bandwidth can increase the data transmission rate. Therefore, mobile communication systems usually use broadband signals to meet the needs of high-speed data transmission. However, when the signal bandwidth exceeds the coherence bandwidth of the channel, the fading characteristics of the channel for different frequency components are no longer the same, resulting in frequency-selective fading. This effect causes inter-symbol interference (ISI), making it difficult for the receiver to accurately restore the original signal.

OFDM technology is a high-speed multi-carrier transmission technology, which is an effective modulation technique designed to combat the challenges posed by frequency-selective channels. Serial data is transmitted in parallel through multiple orthogonal subcarriers, and the orthogonality between subcarriers is used to restore the original data of the OFDM signal at the receiving end, thereby improving the utilization of the spectrum. For an OFDM system with N subcarriers, its modulation process can be considered as multiplying the transmitted signal with the frequency component corresponding to each subcarrier and finally outputting the superposition of time-domain waveforms with different frequency components in the time domain.

Mathematically, the baseband OFDM signal is expressed as:

$$x(t) = \sum_{k=0}^{N-1} X_k e^{j2\pi f_k t} \quad (36)$$

Where X_k is the data sent on the k th subcarrier, and f_k is the frequency component corresponding to the k th subcarrier.

Due to the multipath propagation, the received OFDM baseband signal is the superposition of the transmitted signals from different paths after different time delays. To avoid the ISI, it is usually chosen to add a guard interval at the end of the OFDM symbol, which is usually set to be greater than the channel delay spread to ensure that the OFDM symbols do not overlap at the receiver. Cyclic prefix is the most common way to implement guard interval. Cyclic prefix refers to copying a length from the end of the OFDM symbol and adding it to the starting position to offset the impact of the delayed previous symbol on the next symbol.

After the data is sent, the signal will reach the receiving end, which will sample the transmitted signal according to the sampling frequency. The sequence obtained by sampling is:

$$x(n) = \sum_{k=0}^{N-1} X_k e^{j2\pi f_k n T_s} \quad (37)$$

T_s is the sampling frequency corresponding to the system. The subcarriers of the OFDM system are generally distributed at equal intervals, which can ensure the orthogonality of the subcarriers. The orthogonality of the subcarriers can be used to complete the signal recovery. For the OFDM symbol, the data recovery process on the m th subcarrier is:

$$\sum_{k=0}^{N-1} X_k e^{j2\pi f_k n T_s} e^{-j2\pi f_m n T_s} = \begin{cases} X_k & k = m \\ 0 & k \neq m \end{cases} \quad (38)$$

The subcarriers are strictly orthogonal, so the information carried on other subcarriers will not leak to adjacent subcarriers during the recovery process. The processing flow in the above process is basically the same as the discrete Fourier transform formula. Therefore, in the digital system, the inverse fast Fourier transform (IFFT) and fast Fourier transform (FFT) algorithms can be directly used to modulate and demodulate the OFDM baseband signal, which greatly reduces the difficulty of realizing digital circuits.

OFDM has the ability to mitigate the effects of frequency selective fading. OFDM distributes the data to be transmitted on multiple parallel sub-carriers, ensuring that sub-carriers remain orthogonal and do not interfere with each other. When the symbol duration of each sub-carrier is long enough

such that the data rate per sub-carrier is lower than the channel's coherence bandwidth, the sub-channel experiences frequency-flat fading.

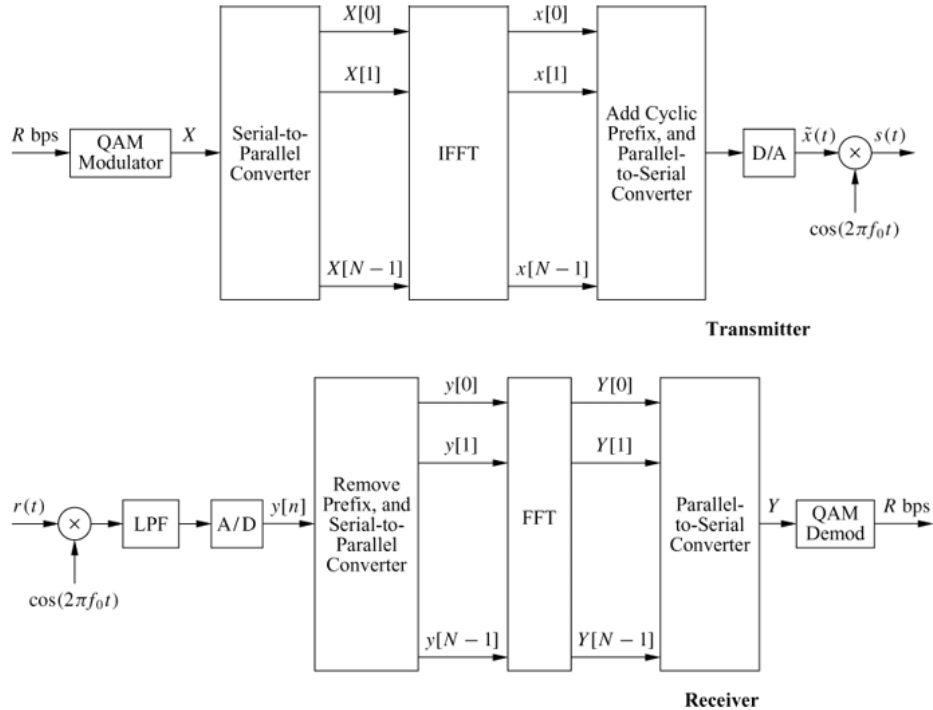


Figure 2. OFDM Transceiver Structure [2].

Figure 2 illustrates the framework of OFDM Transceiver. At the transmitter, the data stream first enters the QAM (quadrature amplitude modulation) module to obtain the signal of each subcarrier. After passing the data through the serial-to-parallel converter, the signal is subjected to an IFFT module to generate the OFDM baseband signal. In order to combat the ISI caused by the multipath effect, a cyclic prefix is added to the baseband signal and then converted back to a serial signal through parallel-to-serial conversion. Finally, after digital-to-analog conversion and mixing with the carrier, the RF transmission signal is generated.

The processing process at the receiver is the opposite of that at the transmitter. The received signal is first mixed with the local carrier, and then the OFDM baseband signal is obtained through a low-pass filter and analog-to-digital converter. After removing the cyclic prefix and performing serial-to-parallel conversion, the parallel signal is subjected to FFT to convert it back to the baseband signal of each subcarrier. After parallel-to-serial conversion, it enters the demodulator and finally recovers the original data stream.

OFDM technology has many advantages: high spectrum efficiency, strong anti-frequency selectivity, and the ability to use IFFT and FFT to achieve fast

modulation and demodulation. It is precisely because of these advantages that OFDM technology is widely used in actual mobile communication systems. It is not only the core technology of 4G but also plays an important role in 5G and future mobile communication systems.

2.3 Carrier Aggregation Technology Overview

This section introduces the basic concept of Carrier Aggregation (CA), including its classification and deployment scenarios. CA is an advanced technology that provides a solution to increase system bandwidth for cellular communication systems. It aggregates two or more carriers together for transmission, thereby obtaining a larger transmission bandwidth, a higher transmission rate, and making full use of more discrete spectrum resources. For example, by combining five component carriers, every 10MHz, we can expand the bandwidth to 50MHz, thereby achieving high data transmission rates. In addition, CA can improve network utilization efficiency and user performance by dynamically allocating all available spectrum [3].

2.3.1 Carrier Aggregation Classification

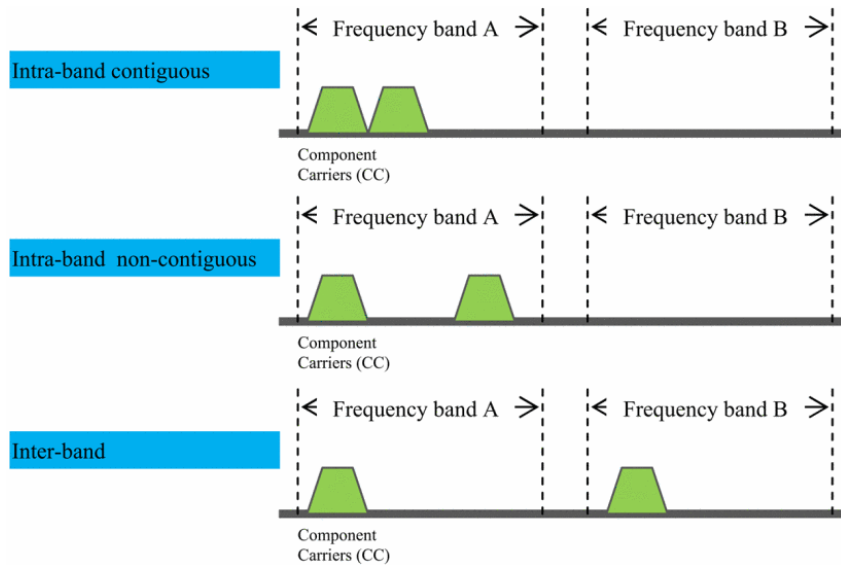


Figure 3: Carrier Aggregation Classification [19].

CA mainly has the 3 forms [19] as Figure 3 shows. The detailed description of 3 carrier aggregation types is as follows.

- Intra-band contiguous Carrier Aggregation: multiple available and adjacent carriers in the same frequency band. When abundant spectrum resources are available, intra-band contiguous CA is a favourable

option, which imposes lower processing requirements on user terminal equipment and facilitates simpler resource allocation.

- **Intra-band non-contiguous Carrier Aggregation:** multiple carriers available in the same frequency band, but they are dispersed. In network deployment, a part of the same frequency band is usually occupied by other communication networks, so the discontinuous idle frequency sub-bands are aggregated in this way.
- **Inter-band Carrier Aggregation:** multiple carriers available in different frequency bands. This method achieves broadband communication through cross-band combination, increasing user flexibility. However, it requires additional complexity in the RF front end of the hardware implementation.

2.3.2 Carrier Aggregation Deployment Scenarios

The following introduces several common deployment scenarios [20] of carrier aggregation technology in detail as Figure 4 shows. For simplicity, there are only two carrier components in each application scenario, and it is assumed that F1 and F2 are two carriers that can be aggregated.

- **Deployment Scenario 1:** carriers F1 and F2 operate within the same frequency band, forming an intra-band CA system, and both carriers are provided by the same base station. Therefore, both carriers experience similar path loss, resulting in largely overlapping coverage areas.
- **Deployment Scenario 2:** Both carriers are provided by the same base station. F1 and F2 operate within the different frequency bands, forming an inter-band CA system. We assume that F2 has a higher frequency, which leads to higher pass loss and smaller coverage. Therefore, the coverage of F2 is contained within that of F1, forming a subset of the F1 coverage area, and CA is provided in the entire coverage of F2.
- **Deployment Scenario 3:** Both carriers are provided by the same base station, as in the previous two scenarios. However, the antennas of F2 are directed toward the cell boundary of F1 (i.e., the antennas of two carriers have different directions), which is designed to improve throughput at the cell boundary. CA is provided in the overlapping area of F1 and F2, rather than across the entire coverage of F1 as in Scenario 2.

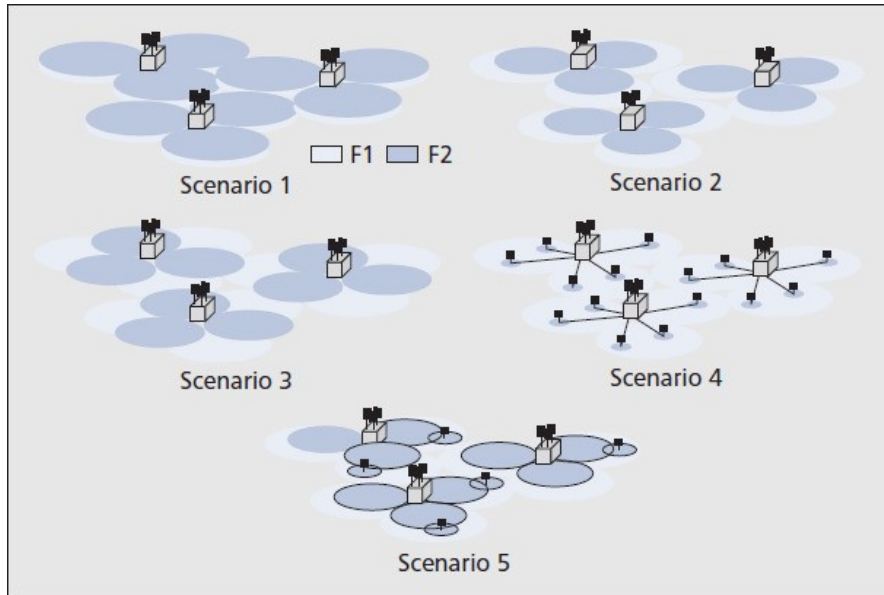


Figure 4. Carrier Aggregation Deployment [20].

- Deployment Scenario 4: Unlike the previous three scenarios, F1 and F2 no longer share the same base station. F1 provides macro coverage, while F2 is deployed in hotspot areas with high user density using Remote Radio Head equipment to enhance system throughput. CA can be applied to users located within the overlapping coverage of RRH and macro cells.
- Deployment Scenario 5: This scenario is an enhanced version of Scenario 2. Building upon the original inter-band CA system, a Frequency Selective Repeater is incorporated into F2 to extend its coverage while remaining within the coverage area of F1. As a result, CA is available across the entire coverage area of F2, the same as in Scenario 2.

2.4 Channel Estimation

As mentioned above, due to the influence of the wireless channel, the signal will fade when passing through the wireless channel. The fading and signal loss problems of the wireless channel are relatively serious, and the fluctuation range is large. Therefore, it is necessary to predict and estimate the wireless channel for reliable communication.

Channel estimation technology is a key technology of wireless systems. A high-performance and reliable communication system must estimate the channel response and then equalize the signal according to the estimation

result at the receiving end. OFDM systems usually use pilot-assisted methods to estimate the channel transfer function by inserting known pilot signals in the OFDM resource grid. The pilot-based channel estimation algorithm can better track channel changes and improve system performance [22].

The basic steps of pilot-based channel estimation are:

- (1) Insert the pilot symbol into the specific position of the signal at the transmitter.
- (2) At the receiver, use received signals and the known pilot signals to estimate the channel response at the pilot position.
- (3) Finally use filtering, interpolation and other methods to obtain the channel response in the entire frequency domain and time domain.

Classical methods for estimating the channel response at the pilot position include the least squares (LS) algorithm, the minimum mean square error (MMSE) algorithm and the DFT-based channel estimation algorithm.

2.4.1 Least Square Algorithm

The LS (Least Squares) algorithm is the simplest method among the channel estimation algorithms, which is computationally efficient, and easy to implement. This section presents the derivation of the LS method as follows.

We insert pilot signals into the transmitted OFDM data, and define the transmitted pilot signal as X_p :

$$X_p = \text{diag}[X_p(0), X_p(1), \dots, X_p(N-1)] \quad (39)$$

The received pilot signal is Y_p :

$$Y_p = [Y_p(0), Y_p(1), \dots, Y_p(N-1)] \quad (40)$$

Define the true channel response as H_p , and the additive noise as Z . The relationship between the received signal and the transmitted signal is given by:

$$Y_p = X_p H_p + Z \quad (41)$$

Define the estimated channel response as \hat{H}_{LS} . The goal of the LS method is to minimize the square error of the received signal $J(H_p)$:

$$J(H_p) = \|Y_p - X_p \hat{H}_{LS}\|_2^2 = \left[(Y_p - X_p \hat{H}_{LS})^H (Y_p - X_p \hat{H}_{LS}) \right] \quad (42)$$

By equating the partial derivative of (42) to zero, we can obtain the channel response \hat{H}_{LS} :

$$\hat{H}_{LS} = X_p^{-1} Y_p \quad (43)$$

$$\hat{H}_{LS}[k] = \frac{Y_p(k)}{X_p(k)}, k = 0, 1, 2, \dots, N - 1 \quad (44)$$

From the above expression, it is evident that the LS channel estimation algorithm involves only a single division per subcarrier, which has low computational complexity. However, this method is sensitive to noise because it does not consider the effect of noise.

2.4.2 MMSE Algorithm

The MMSE (Minimum Mean Square Error) algorithm utilizes the prior information of the channel and considers the impact of noise, resulting in better estimation accuracy compared to the LS method. The derivation of the MMSE method is as follows.

The MMSE Error of channel estimation can be expressed as:

$$MSE = \mathbb{E} \left[(H_p - \hat{H})^H (H_p - \hat{H}) \right] \quad (45)$$

where \hat{H} is the estimated channel response, and H_p is the true channel response. The purpose of the MMSE method is to determine a matrix W to make WY_p approaches H_p , which minimizes (45).

Let $\hat{H} = WY_p$ and substitute it into (45), we can get the formula:

$$MSE = \mathbb{E} \left[(H_p - WY_p)^H (H_p - WY_p) \right] \quad (46)$$

To minimize the MSE, let the partial derivative of MSE with respect to W^H be zero, and we can get the estimated channel response:

$$\hat{H} = R_{H_p Y_p} (R_{Y_p Y_p})^{-1} Y_p \quad (47)$$

Where $R_{H_p Y_p}$ is the cross-correlation matrix of H_p and Y_p , $R_{Y_p Y_p}$ is the auto-correlation matrix of Y_p . They can be expressed as (48) and (49):

$$\begin{aligned} R_{H_p Y_p} &= \mathbb{E}(H_p Y_p^H) = \mathbb{E} \left[H_p (X_p H_p + Z)^H \right] \\ &= \mathbb{E}(H_p H_p^H X_p^H + H_p Z^H) \\ &= R_{H_p H_p} X_p^H \end{aligned} \quad (48)$$

$$\begin{aligned} R_{Y_p Y_p} &= \mathbb{E}(Y_p Y_p^H) = \mathbb{E} \left[(X_p H_p + Z)(X_p H_p + Z)^H \right] \\ &= \mathbb{E}(X_p H_p H_p^H X_p^H + X_p H_p Z^H + Z H_p^H X_p^H + Z Z^H) \\ &= X_p R_{H_p H_p} X_p^H + \sigma_N^2 \mathbf{I} \end{aligned} \quad (49)$$

Among them, $R_{H_p H_p} = \mathbb{E}(H_p H_p^H)$ is the autocorrelation matrix of true channel response, σ_N^2 represents the noise variance of the channel, and \mathbf{I} represent the identity matrix. Therefore, equation (47) can be expressed as:

$$\begin{aligned} \hat{H}_{MMSE} &= R_{H_p H_p} X_p^H (X_p \mathbb{E}(H_p H_p^H) X_p^H + \sigma_N^2 \mathbf{I})^{-1} Y_p \\ &= R_{H_p H_p} X_p^H (R_{H_p H_p} + \sigma_N^2 \mathbf{I})^{-1} X_p^{-1} Y_p \\ &= R_{H_p H_p} X_p^H (R_{H_p H_p} + \sigma_N^2 \mathbf{I})^{-1} \hat{H}_{LS} \end{aligned} \quad (50)$$

It can be observed that the MMSE algorithm is found on the LS algorithm and takes the influence of noise into consideration. Therefore, its estimation performance is usually superior to that of the LS method. In OFDM systems with cyclic prefixes, the frequency domain channel matrix is a diagonal matrix, making the matrix inversion operation can be performed with relatively low complexity. Nevertheless, obtaining the prior knowledge $R_{H_p H_p}$ remains a challenge in practise [9].

2.4.3 DFT-Based Channel Estimation Algorithm

The channel estimation algorithm based on discrete Fourier transform (DFT) has important application value in OFDM systems. The algorithm achieves an effective trade-off between performance and complexity between the LS method and the MMSE method. LS algorithm is simple to calculate, but it is sensitive to noise and has relatively low estimation accuracy. In contrast, the MMSE algorithm shows good performance in a noisy setting, yet it suffers from high computational complexity, making it hard to satisfy real-time requirements. The DFT-based method can improve the accuracy compared with the LS method while ensuring low computational complexity through joint processing of the frequency domain and time domain [23].

In OFDM systems, the guard interval between each OFDM symbol is usually designed to be greater than the channel delay spread to ISI. The channel impulse response typically exhibits a concentrated distribution characteristic in the time domain due to the multipath effect. Most of the energy is concentrated around the dominant propagation paths, which may correspond to the first few specific sampling points, while the energy at other locations is relatively small [24][25]. This energy concentration characteristic provides an important theoretical basis for the DFT-based method.

The core idea of the DFT-based method is to suppress noise by converting the frequency domain and time domain, taking advantage of the characteristic that the channel energy is concentrated in a few specific sampling points. Define \hat{H} as the channel estimate of an OFDM symbol with N subcarriers, obtained by the LS channel estimation algorithm. Taking the IDFT of the channel estimate:

$$IDFT(\hat{H}) = h[n] + z[n] \triangleq \hat{h}[n], n = 0, 1, \dots, N - 1 \quad (51)$$

where $z[n]$ donates the noise component of the time domain. In time-domain representation, the energy of the channel response is mainly concentrated in the first few sampling points, while the noise is evenly distributed throughout the time-domain response. Based on this characteristic, the algorithm sets a threshold and sets the sampling points with lower energy to zero, thereby effectively suppressing the interference of noise. Define the threshold of channel delay as L , the operation of this step can be expressed as.

$$\hat{h}_{DFT} = \begin{cases} h[n] + z[n], & n = 0, 1, 2, \dots, L - 1 \\ 0, & otherwise \end{cases} \quad (52)$$

Then, DFT is applied to the remaining L sequence to convert the processed time domain response back to the frequency domain:

$$\hat{H}_{DFT}[k] = DFT(\hat{h}_{DFT}) \quad (53)$$

Note that the maximum channel delay L should be known in advance. In a low signal-to-noise ratio environment, this algorithm can effectively improve system performance and has important practical application value.

3 Wideband Channel Estimation Framework

3.1 Problem Formulation

This section details the specific scenarios encountered in the wideband channel estimation algorithm and the challenges associated with its implementation. Subsequently, the basic structure of the algorithm is introduced.

3.1.1 Channel Estimation in Carrier Aggregation Systems

Assume that there is an Intra-band non-contiguous CA system, and we have obtained a set of channel estimates $H_i, i = 1, 2 \dots K$ at discrete frequency band through K narrowband receiver. We aim to estimate the channel response $\hat{H}(f^*)$ in these unknown frequency bands that exist between the known frequency bands f^* as figure 5 shows.

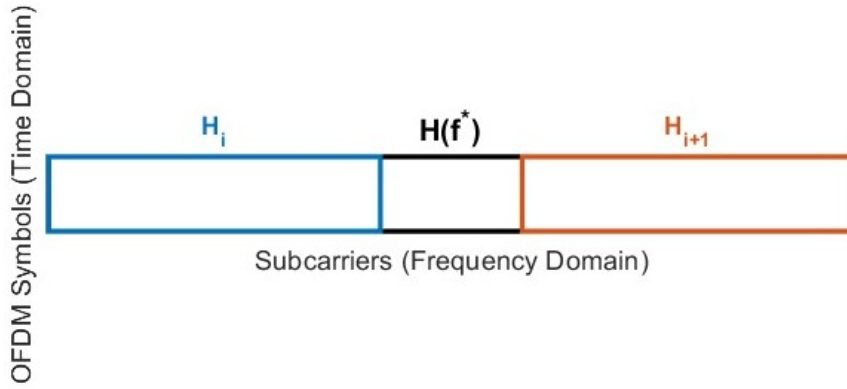


Figure 5. Channel Estimation of Frequency Bands f^*

To evaluate the performance of an interpolation method, we define an error metric based on the relative difference between the interpolated channel estimate and the true channel response. In this thesis, we use the minimum mean square error (MSE) to provide error measure of wideband channel estimates. The interpolation error of a channel block can be expressed as:

$$MSE = \frac{1}{N} \sum_{k=1}^N |\mathbf{H}_{estimated,i} - \mathbf{H}_{true,i}|^2 \quad (54)$$

where $H_{true,i}$ represents the true value of channel response at the i -th frequency band, $\mathbf{H}_{estimated,i}$ is the corresponding estimated channel response. N

donates the total number of elements of the channel matrix, and k represents the index of sampling points.

3.1.2 Phase Discontinuity in Carrier Aggregation Systems

When a receiver changes its operation frequency, the Local Oscillator (LO) will be subject to a random phase offset since the phase-locked loop (PLL) will experience a transient process. In carrier aggregation implementations, each receiver has an independent LO and PLL, and there is no inherent phase synchronization between them [26][27][28]. These factors result in independent phase offsets across frequency bands, leading to phase discontinuities when combining the estimated channels. The following content describes the phenomenon of phase discontinuity in detail.

Let $H_1(f)$ and $H_2(f)$ be the channel estimate of two aggregated bands, measured separately. The corresponding phase responses are:

$$\begin{aligned}\phi(f_1) &= \angle H(f_1) \\ \phi(f_2) &= \angle H(f_2) + \Delta\theta_{\text{offset}}\end{aligned}\tag{55}$$

where $\Delta\theta_{\text{offset}}$ represents the unknown phase offset introduced by LO returning.

Figure 6 shows the frequency response of two adjacent frequency bands without phase shift. It is obvious that band 1 and band 2 are connected smoothly.

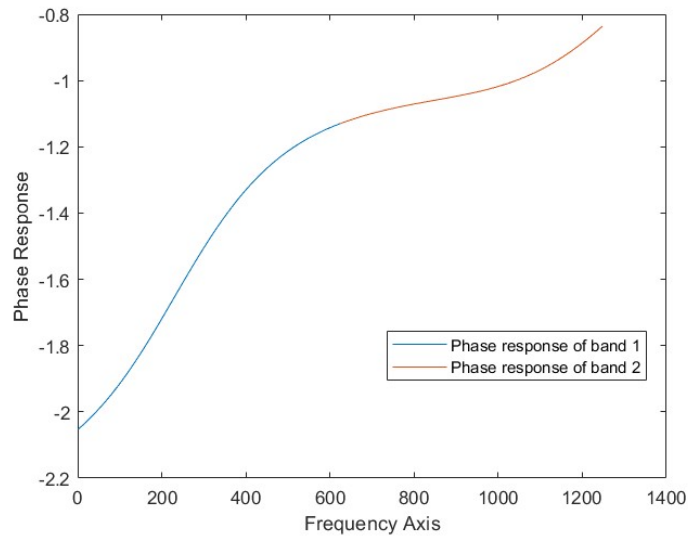


Figure 6. Frequency Response without Phase Offset

Figure 7 shows the frequency response of two adjacent frequency bands, where band 2 has the random frequency offset caused by LO. Band 1 and band 2 are obviously discontinuous. The phase response of band 2 is shifted by $\Delta\theta_{\text{offset}}$.

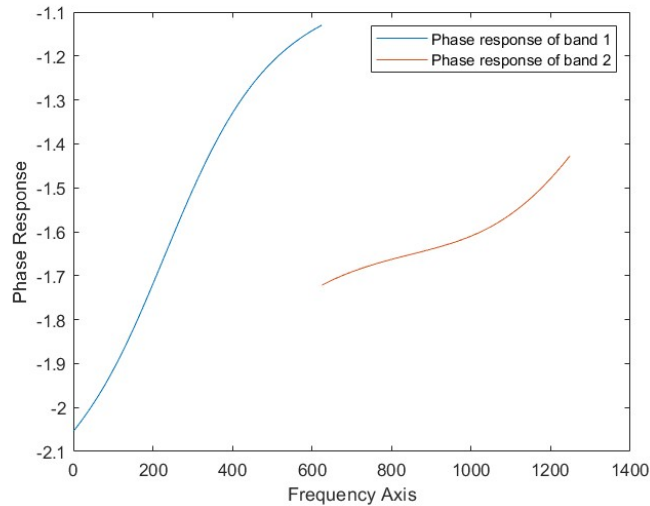


Figure 7. Phase Discontinuity of Carrier Aggregation

This phase offset creates a discontinuity between the two bands, making direct interpolation inaccurate. Therefore, phase correction algorithm must be performed after getting the narrowband channel estimate.

3.1.3 General Structure of Wideband Channel Estimation

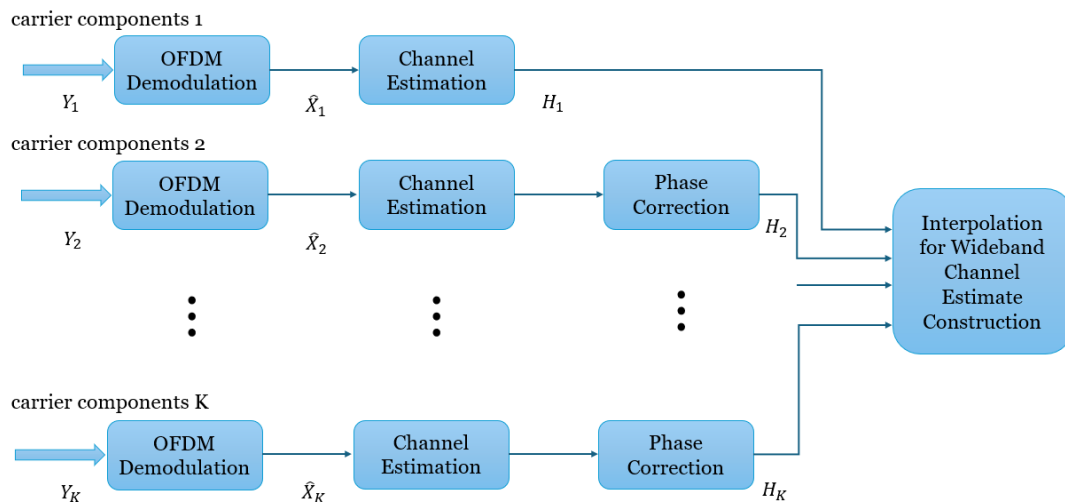


Figure 8. General Structure of Wideband Channel Estimation

The wideband channel estimation algorithm of this thesis involves multiple steps to reconstruct the full-channel response across non-contiguous frequency bands. The estimation process includes OFDM signal reception, narrowband channel estimation, phase offset correction, and interpolation for wideband channel construction. Figure 8 illustrates the general structure of the proposed algorithm.

The algorithm begins with the reception of OFDM signals, followed by narrowband channel estimation for carrier components. Due to potential phase discontinuities between different bands, phase offset correction is applied to ensure phase continuity. Finally, an interpolation process is performed to construct a complete wideband channel estimate from the narrowband estimates. The following sections provide a detailed explanation of each step.

1. OFDM signals reception

Receivers of each carrier component convert the RF signal to the baseband signal. The received baseband signal is processed through an OFDM demodulator using the FFT to transform it into the frequency domain.

The received OFDM symbols at subcarrier k in frequency band i can be expressed as:

$$Y_i(k) = H_i(k)X_i(k) + N_i(k) \quad (56)$$

Where $Y_i(k)$ is the received symbol, $H_i(k)$ is the channel response, $X_i(k)$ is the transmitted symbol, and $N_i(k)$ is the additive noise.

2. Narrowband Channel Estimation

The narrowband channel response of each narrow band H_i can be estimated by the channel estimation algorithms in 2.4. The result is a set of narrowband channel estimates at discrete frequencies.

3. Phase Offset Correction

Because of the phase discontinuity discussion in 3.1.2, a phase correction algorithm should be implemented to ensure phase continuity across frequency bands.

$$H_{correct,i} = H_i \times e^{-j\Delta\theta_{offset}} \quad (57)$$

where $H_{correct,i}$ is the corrected channel response at frequency band i , and $\Delta\theta_{\text{offset}}$ is the estimated phase shift obtained by the phase correction algorithm, which will be introduced in 3.2.

4. Interpolation for Wideband Channel Estimate Construction

The narrowband channel estimates of each carrier component need to be interpolated to construct the complete wideband channel response. In this thesis, we utilize the known channel estimates $H_{correct,i}$ and $H_{correct,i+1}$ to estimate the channel response at an unknown frequency f^* , which lies between these two frequency bands.

$$\hat{H}(f^*) = \mathcal{F}(H_{correct,i}, H_{correct,i+1}) \quad (58)$$

Where \mathcal{F} represents the interpolation algorithm. Frequency band i , f^* and frequency band $i + 1$ are adjacent, ensuring continuity in the estimated wideband channel response.

After integrating the interpolated channel estimates with the narrowband channel estimates from individual carrier components, we obtain a continuous and complete wideband channel estimate. This algorithm framework ensures that phase-aligned interpolation is applied to reconstruct an accurate wideband channel estimate across non-contiguous frequency bands.

3.2 Phase Offset Correction

To address the issue of phase discontinuity, this thesis proposes a phase offset correction algorithm based on the continuity of the first-order derivative of the channel phase response [29]. The key idea is that while the phase response itself has a discontinuity due to the random phase offset, the first-order derivative of the phase response should be continuous across frequency bands. By leveraging this property, we can reconstruct a seamless phase response for the entire wideband channel.

We now assume that in a non-contiguous Carrier Aggregation system, the channel responses of sub-bands f_1 and f_2 are obtained by narrowband channel estimation. The frequency band between f_1 and f_2 is f^* . The channel estimate of f_1 has no phase offset, and the channel estimate of f_2 has a phase offset.

Figure 9 shows the process of the phase offset correction algorithm in this thesis. This algorithm interpolates the differential of the phase response of two discontinuous frequency bands and then integrates to obtain a

continuous phase response. Subsequently, subtract the originally measured phase from the reconstructed phase of the second band. Finally, an averaging operation is applied to mitigate errors and estimate the overall phase offset of the second band.

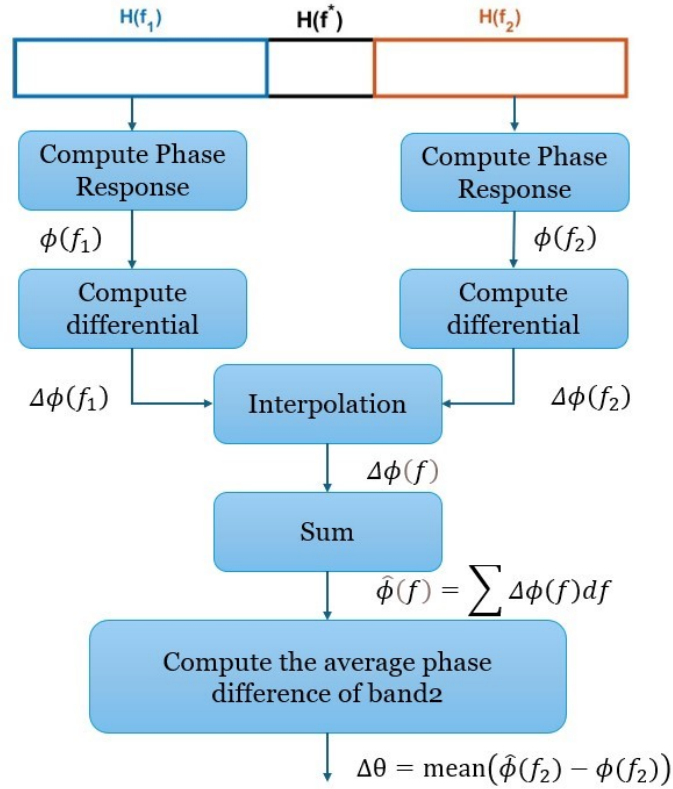


Figure 9. Phase Offset Correction

A detailed description of the steps is provided below:

1. Compute the phase response for each frequency band

Given the channel frequency response $H(f)$ for two bands, extract the phase response using the unwrapped phase function:

$$\phi(f) = \text{unwrap}(\angle H(f)) \quad (59)$$

Therefore, $\phi(f_1)$ and $\phi(f_2)$ represent the phase responses of bands 1 and 2, respectively. The phase of a signal is restricted within $[-\pi, \pi]$, which causes phase discontinuities when phase change exceeds this range. To address this, the unwrapping operation removes these discontinuities to obtain a continuous phase function.

2. Compute the phase response differential

The first-order derivative of the phase response provides a smooth and continuous characteristic. Compute the phase responses differential for both bands.

$$\Delta\phi(f_1) \approx \frac{d}{df} \phi(f_1), \quad \Delta\phi(f_2) \approx \frac{d}{df} \phi(f_2) \quad (60)$$

The discontinuity presents in $\phi(f_2)$ is eliminated in $\Delta\phi(f_2)$, making it suitable for interpolation.

3. Interpolate the differential of the phase response

Given $\Delta\phi(f_1)$ and $\Delta\phi(f_2)$, perform interpolation across the frequency gap to obtain a smooth and unified differential phase response $\Delta\phi(f)$. The interpolation method can be Kriging-based, spline-based, or another suitable technique ensuring a smooth transition. The principle and implementation of the interpolation algorithm will be introduced in 3.3.

4. Calculate the sum to construct the phase response

The phase response for the entire wideband channel is obtained by calculating the sum of interpolated phase response differential:

$$\hat{\phi}(f) = \sum \Delta\phi(f) \quad (61)$$

5. Apply phase correction

Although the phase response has been obtained in the previous step, the integral operation may cause cumulative errors in practice. To reduce the impact of the error, this step implements phase offset correction by performing an overall phase shift on band 2.

Compute the average phase difference between the reconstructed $\hat{\phi}(f_2)$ and the original $\phi(f_2)$:

$$\widehat{\Delta\theta} = \text{mean}(\hat{\phi}(f_2) - \phi(f_2)) \quad (62)$$

Apply a phase shift correction to the original second-band channel response:

$$H^{corrected}(f_2) = H(f_2)e^{-j\widehat{\Delta\theta}} \quad (63)$$

This ensures that the phase response of band 2 is aligned with that of band 1, leading to a seamless wideband channel estimate for the next step.

The algorithm uses the continuity of the differential phase response to effectively correct the phase shift caused by LO switching. The first-order derivative is interpolated and then integrated back to obtain the phase response. After obtaining the average value of the phase shift, the channel estimate is phase corrected. This method ensures that the estimated wideband channel maintains phase continuity in each frequency band, providing a prerequisite for the subsequent interpolation operation of the channel estimate.

3.3 Interpolation for Wideband Channel Reconstruction

In carrier aggregation-based wideband channel estimation, interpolation plays a crucial role in reconstructing the channel response over the entire bandwidth. Since the channel is measured at separate, non-contiguous frequency bands, interpolation methods are needed to estimate the missing frequency components and ensure a continuous and accurate channel response. The selection of an interpolation algorithm impacts the accuracy of the reconstructed channel, as well as the time and resources required for computation.

This section introduces and compares three different interpolation methods: linear interpolation, spline interpolation and Kriging interpolation.

3.3.1 Linear Interpolation

Linear Interpolation is the simplest method, assuming that the function varies linearly between known points. The interpolated value $H(f)$ at unknown frequency f^* is given by:

$$\widehat{H}(f^*) = H(f_i) + \frac{H(f_{i+1}) - H(f_i)}{f_{i+1} - f_i} (f^* - f_i), \quad f_i \leq f^* \leq f_{i+1} \quad (64)$$

Where $H(f_i)$ and $H(f_{i+1})$ are the known data points at f_i and f_{i+1} .

Although computationally efficient, this method can introduce severe errors when the function exhibits significant nonlinear changes. Therefore, linear interpolation is not suitable for channel estimation in most cases.

3.3.2 Spline Interpolation

Spline interpolation is a numerical interpolation method that approximates data points through piecewise polynomial functions. The most common spline interpolation method is cubic spline interpolation, which uses piecewise cubic polynomials to fit data points and ensures the continuity of function values and their first-order and second-order derivatives at the piecewise points.

Assume there are $n + 1$ known data points:

$$(x_0, y_0), (x_1, y_1), \dots, (x_n, y_n) \quad (65)$$

The goal of spline interpolation is to find a set of cubic polynomials $H_i(x)$ that connect these points:

$$H_i(x) = a_i + b_i(x - x_i) + c_i(x - x_i)^2 + d_i(x - x_i)^3 \quad (66)$$

where $x \in [x_i, x_{i+1}]$, and $i = 0, 1, \dots, n - 1$ meaning there are n cubic polynomials.

To ensure smoothness and accuracy, the following constraints must be satisfied:

1. Interpolation Condition:

$$H_i(x_i) = y_i, \quad H_i(x_{i+1}) = y_{i+1}, \quad i = 0, 1, \dots, n - 1 \quad (67)$$

2. First Derivative Condition:

$$H'_i(x_{i+1}) = H'_{i+1}(x_{i+1}), \quad i = 0, 1, \dots, n - 2 \quad (68)$$

3. Second Derivative Condition:

$$H''_i(x_{i+1}) = H''_{i+1}(x_{i+1}), \quad i = 0, 1, \dots, n - 2 \quad (69)$$

4. Boundary Conditions:

$$H''_0(x_0) = 0, \quad H''_{n-1}(x_n) = 0 \quad (70)$$

Which means that the spline has zero curvature at the endpoints.

$$H'_0(x_0) = f'(x_0), \quad H'_{n-1}(x_n) = f'(x_n) \quad (71)$$

This enforces a specified slope at the boundaries.

Taking cubic spline interpolation as an example, derive the calculation process of spline interpolation

Firstly, for each interval $[x_i, x_{i+1}]$, define the Cubic Spline Equations:

$$H_i(x) = a_i + b_i(x - x_i) + c_i(x - x_i)^2 + d_i(x - x_i)^3 \quad (72)$$

Since there are n intervals, we have $4n$ unknowns: a_i, b_i, c_i, d_i .
Determining a_i using Interpolation Condition:

$$a_i = y_i \quad (73)$$

Therefore:

$$b_i h_i + c_i h_i^2 + d_i h_i^3 = y_{i+1} - y_i \quad (74)$$

where $h_i = x_{i+1} - x_i$ is the step size

The second derivative:

$$H_i''(x) = 2c_i + 6d_i(x - x_i) \quad (75)$$

From the second derivative condition we can derive:

$$c_i + 3d_i h_i = c_{i+1} \quad (76)$$

which forms a system of equations for c_i .

Defining $M_i = S_i''(x_i)$, we can get:

$$d_i = \frac{M_{i+1} - M_i}{6h_i} \quad (77)$$

$$c_i = \frac{M_i}{2} \quad (78)$$

According to the interpolation condition (67):

$$y_{i+1} = H_i(x_{i+1}) = a_i + h_i b_i + h_i^2 c_i + h_i^3 d_i \quad (79)$$

Substituting the formula (73), (77), and (78) into (79), and we can derive the expression of b_i :

$$b_i = \frac{y_{i+1} - y_i}{h_i} - \frac{h_i}{2} M_i - \frac{h_i}{6} (M_{i+1} - M_i) \quad (80)$$

In order to solve M_i , we start with the first derivative:

$$\begin{aligned} H'_i(x_{i+1}) &= b_i + 2c_i(x_{i+1} - x_i) + 3d_i(x_{i+1} - x_i)^2 \\ &= b_i + 2c_i h + 3d_i h^2 \end{aligned} \quad (81)$$

$$\begin{aligned} H'_{i+1}(x_{i+1}) &= b_{i+1} + 2c_i(x_{i+1} - x_{i+1}) + 3d_i(x_{i+1} - x_{i+1})^2 \\ &= b_{i+1} \end{aligned} \quad (82)$$

By Substituting (81) and (82) into the first derivative condition:

$$b_i + 2h_i c_i + 3h_i^2 d_i = b_{i+1} \quad (83)$$

Substitute the formula (77) and (80) into (83):

$$h_i m_i + 2(h_i + h_{i+1}) m_{i+1} + h_{i+1} m_{i+2} = 6 \left[\frac{y_{i+2} - y_{i+1}}{h_{i+1}} - \frac{y_{i+1} - y_i}{h_i} \right] \quad (84)$$

This leads to a tridiagonal matrix equation:

$$\mathbf{A}\mathbf{M} = \mathbf{B} \quad (85)$$

Where \mathbf{A} is the Tridiagonal Matrix:

$$\mathbf{A} = \begin{bmatrix} 2(h_0 + h_1) & h_1 & 0 & \dots & 0 \\ h_1 & 2(h_1 + h_2) & h_2 & \dots & 0 \\ 0 & h_2 & 2(h_2 + h_3) & \dots & \vdots \\ \vdots & \vdots & \vdots & \ddots & h_{n-2} \\ 0 & 0 & 0 & h_{n-2} & 2(h_{n-2} + h_{n-1}) \end{bmatrix} \quad (86)$$

\mathbf{M} is the vector of the second derivatives:

$$\mathbf{M} = \begin{bmatrix} M_1 \\ M_2 \\ \vdots \\ M_{n-1} \end{bmatrix} \quad (87)$$

\mathbf{B} is the Data-Driven Vector which contains values calculated from known data points:

$$\mathbf{B} = 6 \begin{bmatrix} \frac{y_2 - y_1}{h_1} - \frac{y_1 - y_0}{h_0} \\ \frac{y_3 - y_2}{h_2} - \frac{y_2 - y_1}{h_1} \\ \vdots \\ \frac{y_n - y_{n-1}}{h_{n-1}} - \frac{y_{n-1} - y_{n-2}}{h_{n-2}} \end{bmatrix} \quad (88)$$

After calculating M_i , we can get the spline coefficient:

$$c_i = \frac{M_i}{2}, \quad d_i = \frac{M_{i+1} - M_i}{6h_i}, \quad b_i = \frac{y_{i+1} - y_i}{h_i} - \frac{h_i}{3}M_{i+1} - \frac{h_i}{6}M_i \quad (89)$$

Therefore, for a given unknown point x^* in the interval $[x_i, x_{i+1}]$, the interpolation value is given by equation (66):

$$H_i(x^*) = a_i + b_i(x^* - x_i) + c_i(x^* - x_i)^2 + d_i(x^* - x_i)^3 \quad (90)$$

3.3.3 Kriging Interpolation

Although spline interpolation can ensure good smoothness, it has limitations when processing channel data with complex spatial correlation. Spline interpolation is mainly based on the geometric position of data points for fitting and does not consider the physical statistical characteristics behind the data.

Kriging interpolation is a regression algorithm that interpolates random processes based on covariance functions, and is an implementation of best linear estimation (BLE). It combines known data points in a linear manner. On the basis of satisfying unbiasedness, it achieves an estimation with the minimum variance by optimizing the weights [30]. Therefore, it can better adapt to the complex and changeable characteristics of wireless channels and provide estimation results that are more in line with the actual channel state.

The following is the derivation of the kriging algorithm:

Kriging method assumes that the interpolated value at an unknown point x^* , denoted as $\hat{H}(x^*)$ is a linear combination of the observed values at known points x_1, x_2, \dots, x_K :

$$\hat{H}(x^*) = \sum_{i=1}^K \lambda_i H(x_i) \quad (91)$$

where K is the number of known data points, λ_i are the interpolation weights, and $H(x_i)$ are the observed values at known data points.

Define the interpolation error as:

$$e(x^*) = H(x^*) - \hat{H}(x^*) \quad (92)$$

The mean squared error (MSE) is given by:

$$\begin{aligned} E[e^2(x^*)] &= E \left[\left(H(x^*) - \sum_{i=1}^K \lambda_i H(x_i) \right)^2 \right] \\ &= E[H^2(x^*)] - 2 \sum_{i=1}^K \lambda_i E[H(x^*)H(x_i)] \\ &\quad + \sum_{i=1}^K \sum_{j=1}^K \lambda_i \lambda_j E[H(x_i)H(x_j)] \end{aligned} \quad (93)$$

To minimize the error, take the derivative with respect to λ_i :

$$\frac{\partial E[e^2(x^*)]}{\partial \lambda_i} = -2C(x^*, x_i) + 2 \sum_{j=1}^K \lambda_j C(x_i, x_j) = 0 \quad (94)$$

Where $C(x_i, x_j)$ is the covariance coefficient of $H(x_i)$ and $H(x_j)$. $C(x^*, x_i)$ is the covariance coefficient of $H(x^*)$ and $H(x_i)$.

Rearranging:

$$\sum_{j=1}^K \lambda_j C(x_i, x_j) = C(x^*, x_i), \quad i = 1, 2, \dots, K \quad (95)$$

Define C_{known} as the $K \times K$ covariance matrix of known points:

$$C_{\text{known}} = \begin{bmatrix} C(x_1, x_1) & C(x_1, x_2) & \dots & C(x_1, x_K) \\ C(x_2, x_1) & C(x_2, x_2) & \dots & C(x_2, x_K) \\ \vdots & \vdots & \ddots & \vdots \\ C(x_K, x_1) & C(x_K, x_2) & \dots & C(x_K, x_K) \end{bmatrix} \quad (96)$$

C_{cross} as the $K \times 1$ covariance vector between known points and the unknown point:

$$C_{cross} = \begin{bmatrix} C(x^*, x_1) \\ C(x^*, x_2) \\ \vdots \\ C(x^*, x_K) \end{bmatrix} \quad (97)$$

λ as the weight vector:

$$\lambda = \begin{bmatrix} \lambda_1 \\ \lambda_2 \\ \vdots \\ \lambda_K \end{bmatrix} \quad (98)$$

Then, the system of equations can be written as:

$$C_{known}\lambda = C_{cross} \quad (99)$$

Solving for λ :

$$\lambda = C_{known}^{-1}C_{cross} \quad (100)$$

The interpolated value is computed as:

$$\hat{H}(x^*) = \lambda^T H_{known} \quad (101)$$

Where H_{known} is the vector of the observed point:

$$H_{known} = [H(x_1) \quad H(x_2) \quad \cdots \quad H(x_K)] \quad (102)$$

Kriging interpolation provides a statistically optimal estimation approach by leveraging the correlation properties of the data and minimizing estimation variance. However, prior knowledge of the correlation matrix is required for Kriging interpolation. An inaccurate correlation model can significantly degrade its performance. In contrast, spline interpolation constructs an interpolation function by ensuring local smoothness and satisfying given interpolation constraints, without the need for precise prior knowledge about correlations matrix [31].

4 Simulation Results and Performance Evaluation

The preceding chapters provided background knowledge and a theoretical framework for the carrier aggregation based wideband channel estimation and phase correlation algorithm.

In this chapter, we introduce the MATLAB simulation of wideband channel estimation of this thesis and then evaluate its performance. First, we describe the simulation setup, including the system parameters, channel models, and the methodology for obtaining narrowband channel estimates. Then, this thesis introduced the method of channel response covariance matrix generation methods, and compare different interpolation methods, finding the best length of interpolation algorithm. Finally, we combine the interpolated and corrected narrowband estimates to construct the full wideband channel estimate and evaluate its overall accuracy.

4.1 Simulation Setup

This section outlines the simulation framework used to evaluate wideband channel estimation via carrier aggregation and interpolation. The simulation aims to generate a wideband channel and extract the narrowband components corresponding to multiple carrier components to generate the corresponding narrowband channel. Then, OFDM signals is transmitted, and the wideband channel estimation algorithm is implemented.

4.1.1 Channel Generation

In the simulation of this thesis, a channel generator is designed to generate the wideband channel and corresponding narrowband channel for signal transmission and performance evaluation. The Channel Generator contains two parts: wideband channel generation and narrowband channel extraction.

To generate the wideband signal, this thesis configures an NR carrier with a system bandwidth of 49.5MHz , which corresponds to 275 resource blocks (RBs), where each RB consists of 12 subcarriers, and the subcarrier spacing is 15KHz . To simulate multipath propagation effects, we configure a Tap Delay Line (TDL) channel model with TDL-C profile, which is commonly used to represent non-line-of-sight propagation [32]. Table 1 shows the key parameters of the wideband channel configuration.

Carrier Frequency	3GHz
System bandwidth	49.5MHz
Subcarrier spacing	15KHz

Channel model	TDL-C
Delay spread	10ns
Max Doppler shift	10HZ

Table 1: Wideband Channel Configuration

The wideband channel $H_{wideband}$ is finally generated by MATLAB's perfect channel estimation function, which generate the channel response matrix according to the channel configuration we discuss. In this thesis, $H_{wideband}$ is a 3300×140 matrix, which means that the frequency axis has 3300 subcarriers and the time axis has 140 OFDM symbols.

To ensure the accuracy of the interpolation result during the channel interpolation operation, the frequency separation of the two carrier components should be small enough so that the two carrier components have a high phase correlation. So, we set the bandwidth of the narrowband channels as $9.36MHz$, which corresponds to 624 subcarriers. There are 4 carrier components in this system, all of which are covered by the wideband channel $H_{wideband}$. Multiple narrowband channels $H_{sub}\{i\}, i = 1, 2, 3, 4$ are obtained by extracting 624×140 cells of the wideband channel matrix $H_{wideband}$ as the figure 10 shows:

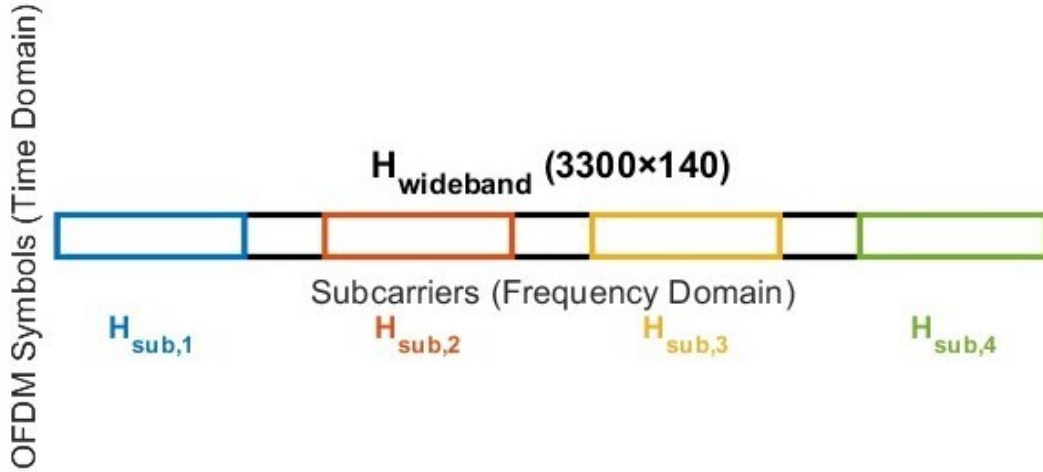


Figure 10. Extraction of Narrowband Channel Models from Wideband Channel

The narrowband channels H_{sub} are used for the signal transmission simulation, which will be introduced in the next section. The spacing between the five narrowband channels is the same. So, there are 3 intervals that need to be filled by the interpolation algorithm, and the bandwidth of each interval is $4.02MHz$, which corresponds to 268 subcarriers.

4.1.2 Signal Transmission and Reception

Firstly, we allocate the DM-RS blocks to the OFDM resources grid to ensure the accuracy of channel estimation and data demodulation. After OFDM modulation and demodulation, we restore the transmission resource grid X_i :

$$X_i \in \mathbb{C}^{N_c \times N_s} \quad i = 1, 2, \dots, 4 \quad (103)$$

Where N_c is the number of subcarriers, and N_s is the number of OFDM symbols. For the considered system, these parameters are set to $N_c = 624$, and $N_s = 140$ respectively.

After OFDM demodulation, the narrowband channel response H_{sub} is applied to the received signal X_i . By performing element-wise multiplication of resource grid X_i and corresponding narrowband channel H_{sub} , the signal transmission in the TDL channel is simulated. Therefore, the received resources grid of each narrowband channel can be expressed as:

$$X_{received,i} = X_i \circ H_{sub}\{i\} \quad i = 1, 2, \dots, 4 \quad (104)$$

4.1.3 Wideband Channel Estimation Implementation

The Least Squares (LS) channel estimation method is employed to acquire the channel response for each carrier component. The estimation process utilizes known reference symbols within the received signal grid to estimate the channel transfer function for each carrier aggregation band. Then, random phase offsets are added to each carrier component independently, which closely simulates the phase offset that occurs at the receiving end due to the LO returning.

Following the initial estimation, the phase correction algorithm (as described in section 3.2) is implemented to maintain phase consistency across different bands. This crucial step addresses phase discontinuities of carrier aggregation systems.

Subsequently, the estimated narrowband channels undergo interpolation to effectively fill the frequency gaps between carrier aggregation bands. The interpolation algorithm ensures smooth transitions between adjacent bands and provides a reliable approximation of the true wideband channel response.

4.2 Covariance Matrix Generation for Kriging Interpolation

In the interpolation approach, the Kriging method relies on an accurate covariance matrix to model the correlation among channel estimates at different frequencies. This section details the methodology for generating the covariance matrix based on Monte Carlo method and the method based on Gaussian Process Regression (GPR) model.

The expression for the covariance matrix is given by [33]:

$$C = \mathbb{E}[hh^H] + \sigma^2 \mathbf{I} \quad (105)$$

where h accounts for the channel response, and $\sigma^2 \mathbf{I}$ represents the noise variance term. Because the estimated narrowband channel probably contains noise, so we need to add the noise variance term to guarantee the accuracy of the covariance matrix.

4.2.1 Monte Carlo Method

Monte Carlo simulation is a statistical technique that relies on repeated random sampling to approximate the expected behaviour of a system. To obtain an empirical covariance matrix for the Kriging interpolation, we simulate the wideband channel generation multiple times and accumulate the correlation information across iterations. Following are the steps of covariance matrix generation:

- (1) **Wideband Channel Sample Generation:** Each wideband channel sample is obtained using the method described in 4.4.1.
- (2) **Mean Computation:** The mean channel response is computed across all Monte Carlo realizations to ensure proper normalization.
- (3) **Accumulation of Centralized Outer Products:** The outer product of the mean-centred channel response vector with its transpose is computed and summed over N iterations to capture the statistical correlation.
- (4) The final covariance matrix is obtained by averaging over N iterations to get $\mathbb{E}[hh^H]$ and then adding noise variance term $\sigma^2 \mathbf{I}$.

By leveraging Monte Carlo simulations, the estimated covariance matrix becomes more reliable as the number of iterations increases. In this thesis, we set the times of iteration N as 1000 for both mean computation and accumulation of outer products, which ensures statistical stability and accuracy in estimating the covariance structure of the wideband channel.

4.2.2 Method based on Gaussian Process Regression Model

In this section, we introduce the Gaussian Progress Regression Model to generate the covariance matrix of the channel response. Different from the Monte Carlo method with a large number of random simulations mentioned above, this method is data-driven and constructs the covariance matrix of the channel by learning from a relatively small number of sample data. The following is the process of method based on GPR model:

- (1) First, we use the same method as before to generate N wideband channels. Since GPR can only process real-valued targets, this thesis extracts the real part of the channel response for training.
- (2) Then, we use the GPR model to train the data. This thesis uses the normalized frequency domain sampling point as the input feature and the real part of the channel response as the output variable for GPR training. We use the commonly used Squared Exponential Kernel as the kernel function, which is defined as [31]:

$$k(x_i, x_j) = \sigma^2 \exp\left(-\frac{(x_i - x_j)^2}{2l^2}\right) \quad (106)$$

where x_i and x_j represent the i -th and j -th frequency sampling points. σ^2 is the signal variance corresponding to the kernel function. l is the scale parameter that controls the smoothness of the function.

- (3) After the training is completed and the GPR model is obtained, the covariance matrix in the frequency dimension can be constructed according to its kernel function definition. Assuming the frequency sampling point set is $\{x_1, x_2, \dots, x_M\}$, the covariance matrix \mathbf{C} can be calculated by the following formula, which is determined by the kernel function:

$$\mathbf{C}(i, j) = \sigma^2 \exp\left(-\frac{(x_i - x_j)^2}{2l^2}\right) \quad (107)$$

4.3 Selection of Suitable Number of Sample Points for Interpolation

In this section, we aim to determine the suitable number of known sampling points for error convergence in interpolation. Specifically, when the number of sampling points is less than this threshold, the error will decrease significantly as the number of sampling points increases; but once this point is

reached, the further increase in the number of sampling points makes the decrease in error negligible, and the error enters a state of convergence.

In the process of wideband channel estimation, interpolation is required in both phase correction and final broadband channel construction. Therefore, it is very important to find the minimum number of points, which can ensure the accuracy of the interpolation algorithm while avoiding unnecessary increases in computing time.

4.3.1 Interpolation of Perfect Channel Estimate

This section investigates the use of kriging and spline interpolation to interpolate the perfect channel estimate to construct a wideband channel estimate. We aim to determine the optimal number of sampling points required for accurate channel response construction. Among them, kriging interpolation uses two different channel covariance matrices, one is generated by the Monte Carlo method in 4.2.1, and the other is generated by the GPR model-based method in 4.2.2. We will also compare the impact of the channel covariance matrices generated by the two methods on kriging interpolation.

In an ideal scenario, the estimated narrowband channel response is obtained without any external noise or estimation error, which is called perfect channel estimation. The interpolation result can be considered as an upper bound for the performance of the wideband channel estimation of this thesis. Since real-world channel estimates inevitably contain errors, understanding the behaviour of interpolation in an idealized setting helps us determine the limits of achievable accuracy.

In this simulation, we only interpolate an unknown gap. As a result, there are two segments of known data: one located to the left of the unknown gap, and the other to the right of the unknown gap. It should be noted that for interpolation of perfect channel estimate, the noise variance term of the covariance matrix is zero: $\sigma^2 = 0$.

The number of known sample points is varied to study its impact on the interpolation accuracy. Specifically, the number of sample points per segment is varied from 2 to 50, and the corresponding interpolation error is computed for both Spline and Kriging methods.

Figure 11 illustrates the comparison of normalized errors between Kriging interpolation and Spline interpolation as a function of the number of sample points. The covariance matrix 1 represents the matrix generated by the Monte Carlo Method in chapter 4.2.1, and the covariance matrix 2 represents the matrix generated by method based on GPR model in chapter 4.2.2. It's

obvious that Kriging interpolation has better performance, with MSE reaching the order of magnitude 10^{-10} . It can be seen that the Kriging method with covariance matrix generated by Monte Carlo method (covariance matrix 1) has the best performance, with the lowest MSE at most points. The Kriging method using the Covariance Matrix generated based on the GPR model method (covariance matrix 2) has a larger error than the former overall, and there is a certain degree of fluctuation.

For the kriging method using covariance matrix 1, the minimum number of known sampling points for error convergence is about 10. At this point, the MSE reaches a very low value. For the Kriging Interpolation with covariance matrix 2, the target number of sampling points for error convergence is about 20. When the number of known points was greater than 20, the error did not decrease significantly.

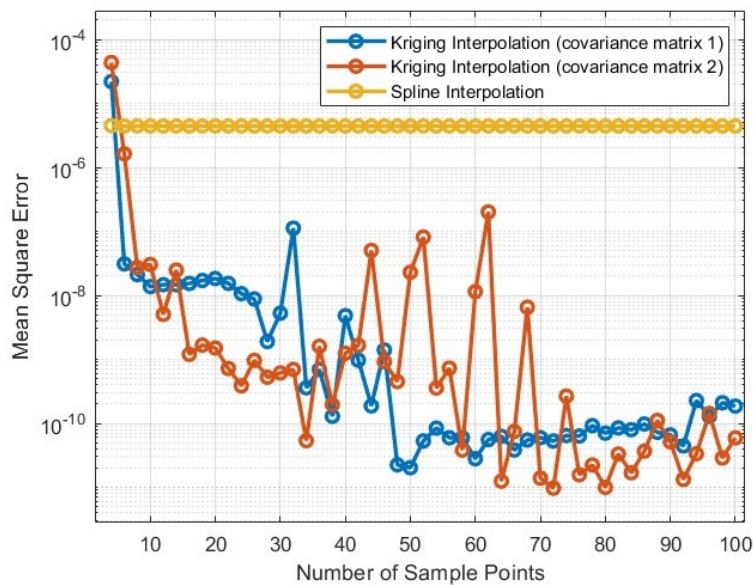


Figure 11. Interpolation Error vs. Number of Sample Points (Perfect Narrowband Channel Estimation)

4.3.2 Interpolation of Imperfect Channel Estimate

In real-world scenarios, narrowband channel estimation is affected by various imperfections, including thermal noise and inaccuracy of estimation algorithms itself. Since the narrowband channel estimate is imperfect, it is essential to evaluate how interpolation techniques perform under practical conditions.

The simulation process of this section is similar to the process of 4.2.2. Figure 12 shows the comparison of mean square errors between Kriging interpolation and Spline interpolation as a function of the number of sample points.

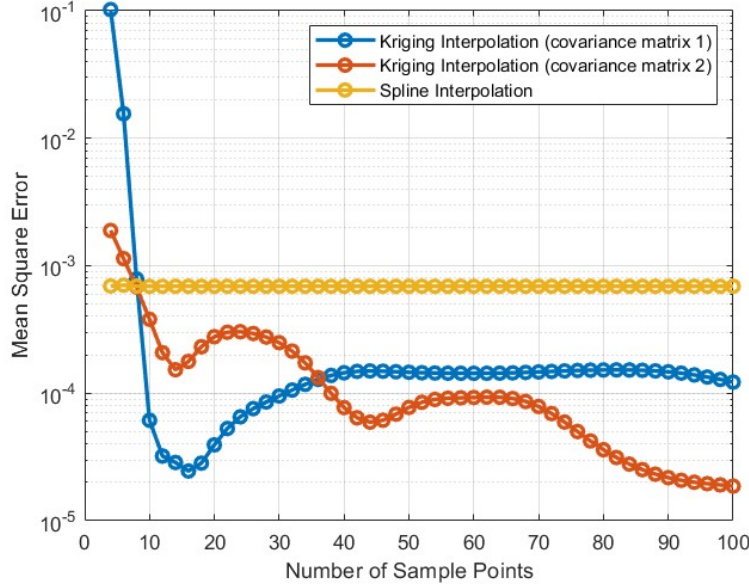


Figure 12. Interpolation Error vs. Number of Sample Points (Imperfect Narrowband Channel Estimation)

For the imperfect channel estimates, kriging methods still have better performance when there are enough sampling points. The kriging method with covariance matrix generated by GPR model performs relatively stable, and the error gradually decreases as the number of sample points increases. The curve of the Kriging method utilizing covariance matrix 1 becomes flat after 40 points.

4.4 Performance of Wideband Channel Estimation

In this section, we aim to evaluate the performance of the wideband channel estimation algorithm. We will first present the performance of the phase correction algorithm and then analyse the overall system performance. The indicators of the evaluation algorithms of the two modules both use the mean square error as defined in (54). We repeated the experiment under different signal-to-noise ratio (SNR) and recorded the mean square error results of the phase correction algorithm and the wideband channel estimation algorithm under each SNR.

Based on the results presented in Section 4.2, we employ the Kriging interpolation method and set the number of sampling points to 40. This

configuration enables the interpolation algorithm to achieve lower estimation error while simultaneously avoiding wasting computing time.

4.4.1 Phase Offset Correction

Our simulations are all carried out in the simulation platform mentioned in Section 4.1. There are 4 narrowband channel estimates for this wideband system. We defined the phase of band 1 as benchmark for the other band, so the phase correction algorithm is applied to bands 2, 3, and 4 sequentially. The phase correction of each frequency band is based on the previous frequency band.

The phase correction results at one time index are shown in Figure 13. From left to right, these are the phases of band 2, band 3, and band 4. The image shows the phase of the perfect channel estimate, the phase of the narrowband channel estimate without correction, and the phase of the narrowband channel estimate after the phase correction. Even though the random phase offset causes a relatively large phase shift in each frequency band, our algorithm successfully corrects the phase offset, making the corrected phase very close to the phase of perfect channel estimates.

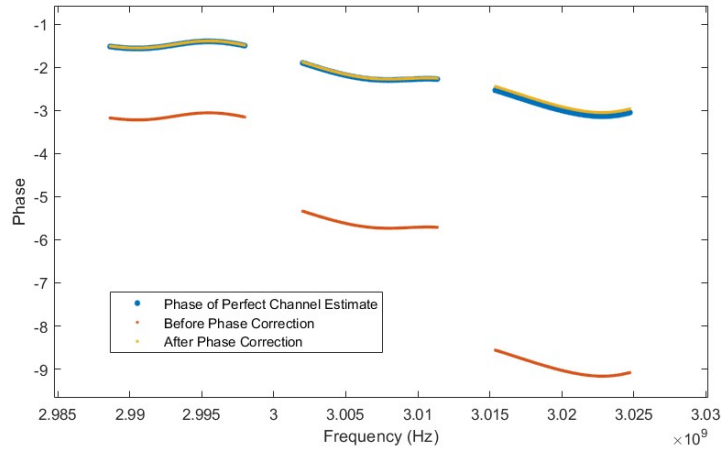


Figure 13. Comparison of Phase before and after Phase Correction

In each SNR case, we perform multiple experiments and take the average to obtain the mean square error of channel estimate after phase offset correction $H_i, i = 1,2,3,4$. Through the error of H_i , we can indirectly evaluate the performance of the phase correction algorithm. Given that the phase of H_1 is set as the phase reference for other bands, its error rate can be used as a reference indicator in the absence of phase offset and is used for comparative analysis with the error rates of Band 2, Band 3, and Band 4. Figure 14 shows the curve of MSE of different frequency bands with SNR.

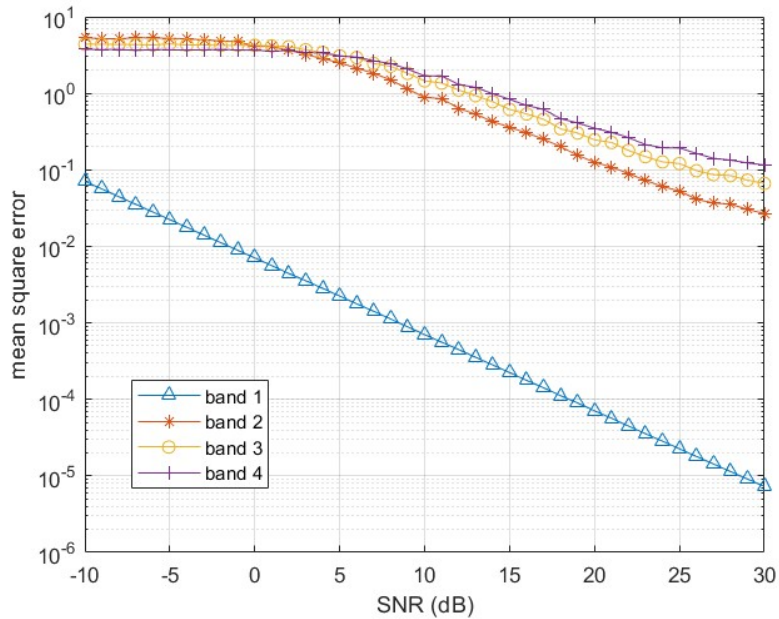


Figure 14. Phase Correction: The MSE curve of different frequency bands with SNR

In the case of high SNR, the phase correction algorithm can effectively control the error of narrowband channel estimates, which below 0.1. Although this error is substantially larger than the error of band 1, it remains within an acceptable range. However, when the SNR is low, the phase correction algorithm demonstrates poor performance, leading to significant errors in the estimated channel responses.

In addition, an increasing trend in the error of H_i is observed from band 2 to band 4 in the high SNR range. This can be attributed to the cumulative effect of errors during the correction process. Specifically, the phase offset of band 3 is estimated based on band 2, and similarly, the correction of band 4 depends on the estimate of band 3. Therefore, any residual error in earlier bands may propagate and amplify in subsequent bands, resulting in a gradual increase in estimation error.

The evaluation of the phase offset correction algorithm shows that it is effective in addressing the phase discontinuity problem in carrier aggregation. Although a cumulative error effect is observed, the phase correction algorithm keeps the error within an acceptable range, which serves as a prerequisite that facilitates the reliable implementation of subsequent channel interpolation operations.

4.4.2 Overall Performance Analysis

In this section, we aim to evaluate the performance of our last module of the wideband channel estimation algorithm: interpolating the narrowband channel estimates after phase correction. As in the previous section, this section also evaluates the performance of the system by calculating the mean square error under different SNR.

The amplitude of the perfect wideband channel estimate, generated based on the parameters and methodology described in Section 4.1.1, is shown in Figure 15.

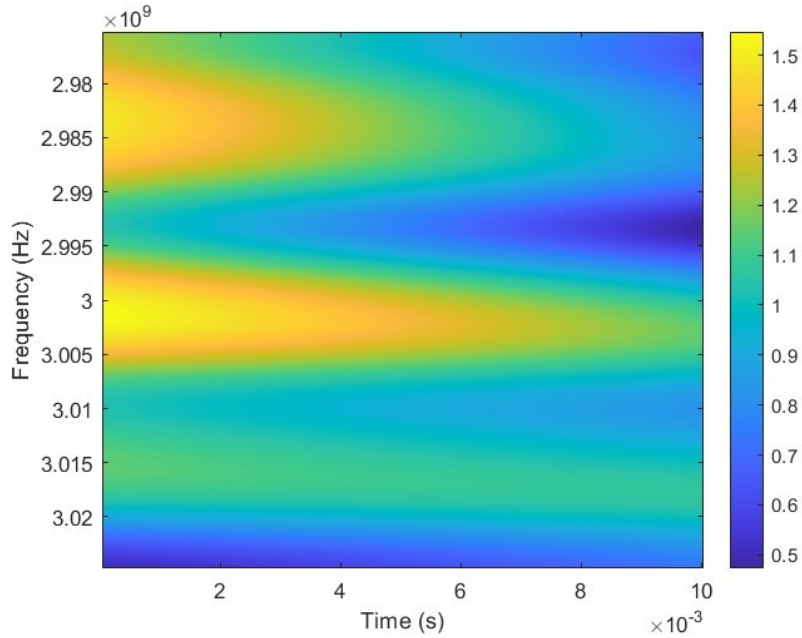


Figure 15. Perfect Wideband Channel Estimate

The amplitude of the constructed wideband channel estimation result at a 30dB SNR is shown in Figure 16. $H_i, i = 1,2,3,4$ are the narrowband channel estimates of each carrier component, and the area pointed by the arrow $G_i, i = 1,2,3$ is the channel estimate obtained by interpolating the gaps between narrowband channel estimates. It can be seen intuitively from this figure that the wideband channel estimates are very close to the actual channel response, indicating that the algorithm of this thesis can successfully construct the wideband channel estimate.

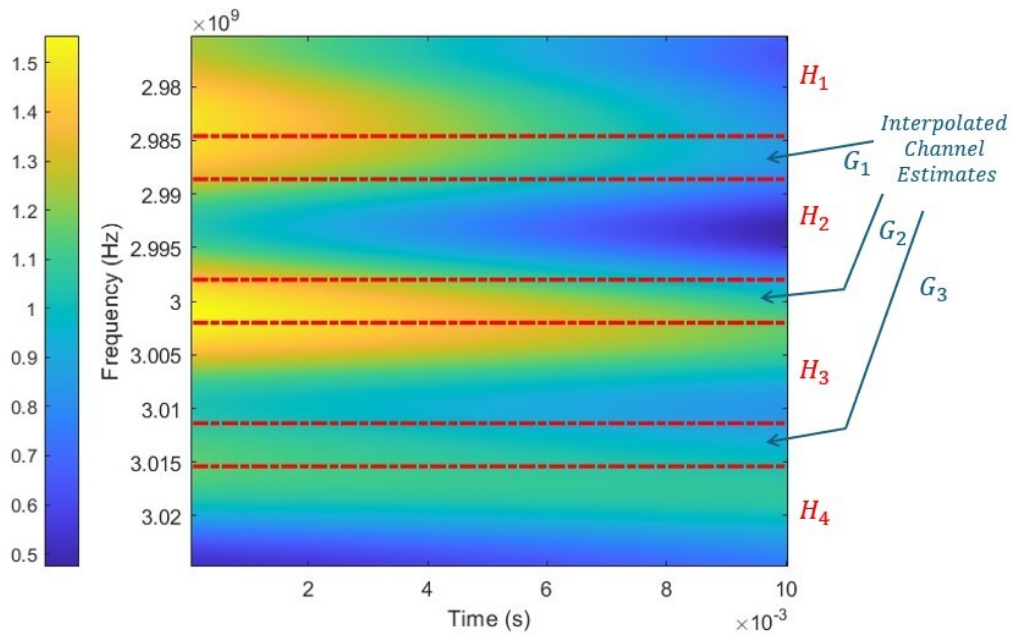


Figure 16. Constructed Wideband Channel Estimate with 30dB SNR

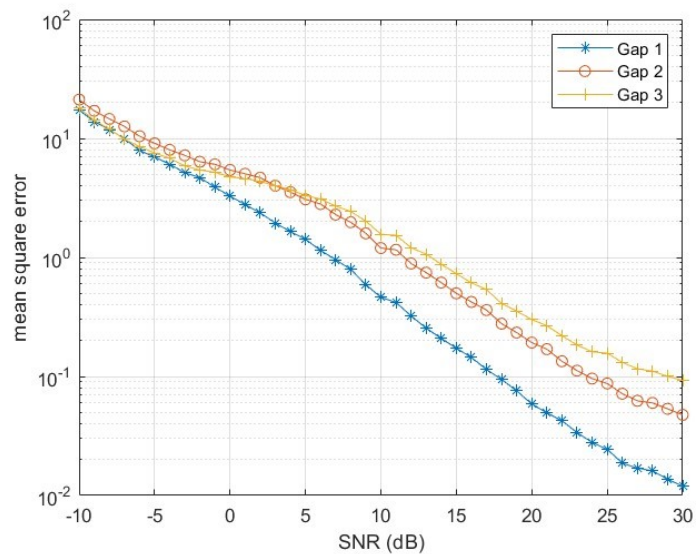


Figure 17. Interpolation: MSE of different frequency gaps varies with the SNR

Figure 17 demonstrates the mean square error for interpolation result of different frequency gaps (G_1 , G_2 and G_3) as a function of SNR. The inaccuracy of the interpolation results in low SNR regions is mainly due to the impaired performance of our phase correction algorithm under such conditions. When the SNR is low, the narrowband channel estimates are significantly biased, which propagates the error throughout the interpolation process, resulting

in significant inaccuracies in the final interpolation results. In the high-SNR regime, the algorithm demonstrates good performance and can achieve relatively small errors. By comparing Figure 17 and Figure 14, we can find that the channel estimates of Gaps obtained by interpolation are close to the channel estimates obtained by the LS algorithm on both sides. This shows that the algorithm has a good performance in the interpolation stage. In addition, there is an error transmission effect in the interpolation stage. It can be clearly seen that for most SNR values, the error of G_3 is greater than that of G_2 , and the error of G_2 is greater than that of G_1 .

5 Conclusions and Future Work

5.1 Conclusions

In this thesis, a wideband channel estimation algorithm using a non-continuous CA system was proposed. The algorithm first estimates the channel of each sub-band in the CA system using the LS method, and then uses the phase offset correction algorithm based on the continuity of the first-order derivative to solve the phase discontinuous problem in the CA system. Finally, the blank spaces between the carrier components are interpolated to obtain the full-band broadband channel estimate of the frequency band covered by this carrier aggregation system.

In the implementation of the interpolation algorithm, this thesis compares the performance of the spline interpolation algorithm and the kriging interpolation algorithm and finds that the kriging interpolation algorithm that uses prior information of the channel performs better than the spline interpolation algorithm. This thesis also finds a suitable number of sample points for interpolation, which allows the interpolation algorithm to maintain high accuracy without consuming unnecessary computing time.

In the simulation of this thesis, a wideband channel with a bandwidth of 49.5MHz was generated. The performance of the proposed wideband channel estimation algorithm was evaluated with a CA-OFDM system consisting of four component carriers, and the bandwidth of each carrier component is 9.36 MHz. The phase offset correction in the algorithm and the final wideband channel estimate construction both showed small errors, which demonstrates the reliability of the wideband channel estimation algorithm of this thesis.

5.2 Future Work

This thesis focused on a specific CA configuration with four component carriers. Future work could generalize the algorithm to support different configurations of carrier components, including different spacing between carrier components and different bandwidths. In addition, alternative channel estimation techniques can be investigated, such as deep learning-based methods, which may improve the estimation accuracy in both narrowband channel estimation stage and interpolation stage.

References

- [1] R. Ratasuk, D. Tolli and A. Ghosh, "Carrier Aggregation in LTE-Advanced," *2010 IEEE 71st Vehicular Technology Conference*, Taipei, Taiwan, 2010
- [2] A. Goldsmith, *Wireless Communications*. Cambridge: Cambridge University Press, 2005.
- [3] G. Yuan, X. Zhang, W. Wang and Y. Yang, "Carrier aggregation for LTE-advanced mobile communication systems," in *IEEE Communications Magazine*, vol. 48, no. 2, pp. 88-93, February 2010.
- [4] H. A. M. Ramli, A. L. Asnawi, F. N. M. Isa and A. W. Azman, "A survey of component carrier selection algorithms for carrier aggregation in long term evolution-advanced," *2017 IEEE 4th International Conference on Smart Instrumentation, Measurement and Application (ICSIMA)*, Putrajaya, Malaysia, 2017.
- [5] W. Xu, S. Shojaei and K. Manolakis, "Carrier-Aggregated Timing Estimation for Radio Positioning," *2019 IEEE 89th Vehicular Technology Conference (VTC2019-Spring)*, Kuala Lumpur, Malaysia, 2019
- [6] M. K. Ozdemir and H. Arslan, "Channel estimation for wireless ofdm systems," in *IEEE Communications Surveys & Tutorials*, vol. 9, no. 2, pp. 18-48, Second Quarter 2007.
- [7] F. Lin, P. -I. Mak and R. P. Martins, "Wideband Receivers: Design Challenges, Tradeoffs and State-of-the-Art," in *IEEE Circuits and Systems Magazine*, vol. 15, no. 1, pp. 12-24, Firstquarter 2015.
- [8] D. Murphy, M. Mikhemar, A. Mirzaei and H. Darabi, "Advances in the design of wideband receivers," *Proceedings of the IEEE 2013 Custom Integrated Circuits Conference*, San Jose, CA, USA, 2013.
- [9] S. Coleri, M. Ergen, A. Puri and A. Bahai, "Channel estimation techniques based on pilot arrangement in OFDM systems," in *IEEE Transactions on Broadcasting*, vol. 48, no. 3, pp. 223-229, Sept. 2002
- [10] O. Edfors, M. Sandell, J. . -J. van de Beek, S. K. Wilson and P. O. Borjesson, "OFDM channel estimation by singular value decomposition,"

- in *IEEE Transactions on Communications*, vol. 46, no. 7, pp. 931-939, July 1998
- [11] J. Li, Z. Zhang, Y. Wang, B. He, W. Zheng and M. Li, "Deep Learning-Assisted OFDM Channel Estimation and Signal Detection Technology," in *IEEE Communications Letters*, vol. 27, no. 5, pp. 1347-1351, May 2023
- [12] Y. Li, H. Minn and R. M. A. P. Rajatheva, "Synchronization, Channel Estimation, and Equalization in MB-OFDM Systems," in *IEEE Transactions on Wireless Communications*, vol. 7, no. 11, pp. 4341-4352, November 2008
- [13] R. Tesi, M. Hamalainen and J. Iinatti, "Channel Estimation Algorithms Comparison for Multiband-OFDM," *2006 IEEE 17th International Symposium on Personal, Indoor and Mobile Radio Communications*, Helsinki, Finland, 2006
- [14] Y. -R. Tsai, C. -C. Wang and X. -S. Li, "Adaptive Channel Estimation for MB-OFDM Systems in Multi-Access Interfering Environments," *VTC Spring 2008 - IEEE Vehicular Technology Conference*, Marina Bay, Singapore, 2008
- [15] B. Su and M. -Y. Wang, "Joint Channel Estimation Methods in Carrier Aggregation OFDM Systems," *2014 IEEE 79th Vehicular Technology Conference (VTC Spring)*, Seoul, Korea (South), 2014.
- [16] W. C. Jakes, Ed., *Microwave Mobile Communications*. New York, NY, USA: Wiley, 1974.
- [17] V. -H. Pham and J. -Y. Chouinard, "A Study on the Channel and Signal Cross Correlation of UHF DTV Channels," *2007 International Symposium on Signals, Systems and Electronics*, Montreal, QC, Canada, 2007.
- [18] R. Zhang, Z. Zhong, Y. Zhang, S. Lu and L. Cai, "Measurement and Analytical Study of the Correlation Properties of Subchannel Fading for Noncontiguous Carrier Aggregation," in *IEEE Transactions on Vehicular Technology*, vol. 63, no. 9, pp. 4165-4177, Nov. 2014
- [19] Iskandar and R. Galih, "Throughput evaluation in LTE-Advanced network access using carrier aggregation," *2015 1st International Conference on Wireless and Telematics (ICWT)*, Manado, Indonesia, 2015.

- [20] Z. Shen, A. Papasakellariou, J. Montojo, D. Gerstenberger and F. Xu, "Overview of 3GPP LTE-advanced carrier aggregation for 4G wireless communications," in *IEEE Communications Magazine*, vol. 50, no. 2, pp. 122-130, February 2012.
- [21] Y. S. Cho, J. Kim, W. Y. Yang, and C. G. Kang, *MIMO-OFDM Wireless Communications with MATLAB*. Singapore: Wiley, 2010.
- [22] Y. R. Zheng and C. Xiao, "Channel Estimation for Frequency-Domain Equalization of Single-Carrier Broadband Wireless Communications," in *IEEE Transactions on Vehicular Technology*, vol. 58, no. 2, pp. 815-823, Feb. 2009.
- [23] Fan Xiang-ning, Leng Bing and Bi Guang-guo, "An improved channel estimation algorithm for OFDM UWB," *Proceedings. 2005 International Conference on Wireless Communications, Networking and Mobile Computing, 2005.*, Wuhan, China, 2005.
- [24] Yang Xiao-dong, Zhu Xiao-ming, Wang Yu-dong and Ma Ning, "Analysis of DFT-based channel estimation algorithm for UWB-OFDM system," *2007 IET Conference on Wireless, Mobile and Sensor Networks (CCWMSN07)*, Shanghai, 2007.
- [25] Y. Kang, K. Kim, and H. Park, "Efficient DFT-based channel estimation for OFDM systems on multipath channels," *IET Communications*, vol. 1, no. 2, pp. 197–202, 2007
- [26] G. Xu and E. C. Kan, "Phase Offset Calibration in Multi-Channel Radio-Frequency Transceivers," in *IEEE Journal of Microwaves*, vol. 4, no. 1, pp. 111-122, Jan. 2024
- [27] D. Vasisht, S. Kumar, and D. Katabi, "Decimeter-level localization with a single WiFi access point," in Proc. 13th USENIX Symp. Netw. Syst. Des. Implementation (NSDI), Santa Clara, CA, USA, Mar. 2016, pp
- [28] M. B. Khalilsarai, S. Stefanatos, G. Wunder and G. Caire, "WiFi-Based Indoor Localization via Multi-Band Splicing and Phase Retrieval," *2019 IEEE 20th International Workshop on Signal Processing Advances in Wireless Communications (SPAWC)*, Cannes, France, 2019

- [29] L. Wang, G. Liu and J. Xue, "Channel Prediction Using a System of Ordinary Differential Equation," *2022 IEEE 22nd International Conference on Communication Technology (ICCT)*, Nanjing, China, 2022
- [30] Y. Gao and T. Fujii, "A Kriging-Based Radio Environment Map Construction and Channel Estimation System in Threatening Environments," in *IEEE Access*, vol. 11, pp. 38136-38148, 2023
- [31] C. E. Rasmussen and C. K. I. Williams, *Gaussian Processes for Machine Learning*. Cambridge, MA, USA: MIT Press, 2006.
- [32] G. -R. Barb, M. Ottesteanu, G. Budura and C. Balint, "Performance Evaluation of TDL Channels for Downlink 5G MIMO Systems," *2019 International Symposium on Signals, Circuits and Systems (ISSCS)*, Iasi, Romania, 2019
- [33] K. Upadhyya., 'Channel Estimation in Large-Scale Multi-Antenna Systems for 5G and Beyond - Novel Pilot Structures and Algorithms' Aalto University publication series DOCTORAL DISSERTATIONS, 138/2018